International Journal of Multiphase Flow 85 (2016) 348–368

Contents lists available at ScienceDirect

International Journal of Multiphase Flow

journal homepage: www.elsevier.com/locate/ijmultiphaseflow

Review

Review on vertical gas–liquid slug flow

A.O. Morgado, J.M. Miranda, J.D.P. Araújo, J.B.L.M. Campos*

Centro de Estudos de Fenómenos de Transporte, Departamento de Engenharia Química, Faculdade de Engenharia da Universidade do Porto, Rua Dr. Roberto Frias, 4200-465 Porto, Portugal

ARTICLE INFO

Article history:
Received 26 April 2016
Revised 15 June 2016
Accepted 3 July 2016
Available online 7 July 2016

Keywords:
Taylor bubble
Gas–liquid slug flow
Vertical columns
Newtonian liquids

ABSTRACT

Vertical slug flow is characterized by the rise of long bullet-shaped gas bubbles with a diameter almost matching that of the tube - Taylor bubbles. Liquid slugs separate consecutive Taylor bubbles, which may interact and coalesce if the distance between them is small. Slug flow has numerous industrial applications, being also observed on physiological and geological systems. In spite of the contribution of the development of non-intrusive experimental techniques to a deeper understanding of slug flow features, the complexity of this flow pattern requires the combined use of numerical approaches to overcome some of the optical problems reported in experimental methods, and other limitations related to the flow aperiodic behavior.

The need to systematize the large amount of data published on the subject and to understand the limitations of the techniques employed constitutes the motivation for this review. In the present work, literature on vertical gas–liquid slug flow, with Newtonian fluids, from 1943 to 2015, covering theoretical, experimental and numerical approaches, is reviewed. Focus is given to single and trains of Taylor bubbles rising through stagnant and co-current liquids.

It should be emphasized, however, that further research still needs to be conducted in some particular areas, namely the hydrodynamics of the liquid film surrounding the Taylor bubbles, the interaction between consecutive bubbles, and a more detailed approach to the flow of Taylor bubbles through co-current liquids.

1. Introduction

When gas and liquid flow simultaneously in a tube, several types of spatial distribution of both phases – flow patterns - may occur depending on the set of fluid properties, flow rates, and on the geometry and inclination of the tube. Realizing the importance of accurately predicting the transition conditions between flow patterns, several authors proposed classifications for upward flow of gas-liquid mixtures in vertical pipes (Barnea, 1987; Hewitt, 1970; Taitel et al., 1980; Taitel and Dukler, 1976). Five main types of gas–liquid flow patterns are usually identified: bubbly, slug, semi-annular, annular, and mist (Fig. 1).

In vertical gas–liquid flow, feeding gas at low flow rates at the bottom of a pipe causes a random distribution of small discrete bubbles through the liquid continuous phase. This behavior, observed both for stagnant and flowing liquid, is designated by bubbly flow (Barnea, 1987; Hewitt, 1970; Moissis and Griffith, 1962; Taha and Cui, 2006; Taitel et al., 1980; Taitel and Dukler, 1976). The increase of the gas flow rate and, consequently, the concentration of small bubbles, promotes coalescence between them, yielding larger bubbles. Named Taylor bubbles after Geoffrey Taylor, a British physicist and mathematician notable for his pioneer work on slug flow (Davies and Taylor, 1950), these large gas bubbles are characterized by their bullet shape: a round-shaped nose followed by a cylindrical main body. Isolated Taylor bubbles rise almost uniformly in vertical pipes, occupying nearly the entire cross-section of the tube. On its turn, continuous slug flow or bubble train flow is characterized by an almost-periodic rise of Taylor bubbles separated by liquid slugs that may contain small, dispersed bubbles in it. Between a Taylor bubble and the tube wall, the liquid flows downwards as a thin falling film. As it reaches the bottom of the bubble, the annular film enters the liquid slug behind it as an expanding jet, with the possibility of creating a recirculation region known as the bubble wake, depending on the flow conditions. Both the shape of the bubble trailing edge and the wake flow pattern depend on the fluid properties and tube geometry, besides flow conditions. If the separation distance between two Taylor bubbles is small enough, the motion and shape of the trailing bubble get largely affected by the flow in the wake of the leading one: the nose becomes distorted and wavy, its velocity increases, and

* Corresponding author.
E-mail addresses: anamorgado@fe.up.pt (A.O. Morgado), jmiranda@fe.up.pt (J.M. Miranda), daraujo@fe.up.pt (J.D.P. Araújo), jmc@fe.up.pt (J.B.L.M. Campos).

http://dx.doi.org/10.1016/j.ijmultiphaseflow.2016.07.002
0301-9322/

Nomenclature

a^2	Specific cohesion m^2
$\dot{b}$	Dimensionless film thickness for turbulent flow
C	Ratio between the centreline and the mean liquid velocities
D	Internal diameter of the tube m
g	Acceleration due to gravity $m\,s^{-2}$
l	Distance between consecutive Taylor bubbles m
l_e	Entrance length m
l_{min}	Minimum separation length for which there is no interaction m
l_s	Length of the liquid slug m
l_{TB}	Length of the Taylor bubble m
l_W	Length of the wake m
r	Radial coordinate m
$\dot{r}$	Distance from the central axis of the tube normalised by its radius m
R	Internal radius of the tube m
R_N	Radius of curvature at the nose of the bubble m
R_{TB}	Taylor bubble radius m
u	Velocity $m\,s^{-1}$
$u*$	Friction velocity $m\,s^{-1}$
U_∞	Velocity of a Taylor bubble rising through stagnant liquid $m\,s^{-1}$
U_C	Maximum or centerline liquid velocity $m\,s^{-1}$
U_F	Velocity in the annular liquid film $m\,s^{-1}$
U_G	Superficial velocity of the gas phase $m\,s^{-1}$
U_l	Velocity of the leading bubble $m\,s^{-1}$
U_L	Mean liquid velocity $m\,s^{-1}$
U_t	Velocity of the trailing bubble $m\,s^{-1}$
U_{TB}	Taylor bubble velocity $m\,s^{-1}$
V_L	Relative liquid velocity in a MFR m^3
V_{TB}	Volume of the Taylor bubble m^3
V_W	Volume of the wake m^3
$\dot{x}$	Axial distance normalised by the tube radius
z	Axial coordinate m
$Z*$	Distance from the nose where the liquid film is fully developed m
Z_A	Interaction distance above the nose of the bubble m

Greek Letters

$\dot{\gamma}$	Deformation rate s^{-1}
δ	Annular liquid film thickness m
μ	Dynamic viscosity Pa s
ρ	Density $kg\,m^3$
σ	Surface tension $N\,m^{-1}$
τ	Shear stress Pa
τ_W	Wall shear stress Pa
υ	Kinematic viscosity $m^2\,s^{-1}$

Dimensionless groups

Ar	Archimedes number
Eo	Eötvös number
Fr	Froude number
M	Morton number
N_f	Inverse viscosity number
Ps	Poiseuille number
Re	Reynolds number
Re_F	Reynolds number based on the velocity of the annular liquid film
Re_{TB}	Reynolds number based on the velocity of the Taylor bubble
Re_{U_L}	Reynolds number based on the mean velocity of the liquid
Re_{V_L}	Reynolds number based on the relative velocity of the liquid in a MFR
We_{U_∞}	Weber number based on the velocity of a Taylor bubble rising through stagnant liquid

List of acronyms

CFD	Computational fluid dynamics
FFR	Fixed frame of reference
MFR	Moving frame of reference
PIV	Particle image velocimetry
PST	Pulsed shadow technique
SFS	Slug flow simulator
VOF	Volume-of-fluid

coalescence between bubbles will occur. In Fig. 2, images of a single Taylor bubble (a) and of two consecutive Taylor bubbles (b) obtained from computational slug flow simulations illustrate the flow details just described.

Coalescence between Taylor bubbles can also result from increasing gas flow rates, leading eventually to the development of semi-annular and annular flow. Semi-annular flow can be seen as an intermediate stage between slug and annular flow, where shorter liquid slugs separate bubbles of increased length. As a consequence of a further increase of the gas flow rate, complete destruction of the liquid slugs occurs and annular flow emerges, *i.e.*, the gas phase becomes a continuum, flowing in the core section of the tube, surrounded by the liquid flowing as a film in the annular space between the gas phase and the tube wall (Hewitt, 1970; Moissis and Griffith, 1962; Taha and Cui, 2006). For even higher gas flow rates, the liquid becomes dispersed within the continuous gas phase in a mist flow.

From the five flow patterns referred, slug flow is usually on the spotlight due to its numerous practical applications. In industrial plants, gas-liquid slug flow is present in vapor-liquid absorbers, vapor generators, reboilers, buoyancy-driven fermenters, vaporizers, and during crystallization (Yun and Shen, 2003), filtration (Mayer et al., 2006) and membrane processes (Bellara et al., 1997; Cui et al., 2003; Ghosh and Cui, 1999; Li et al., 1997; Taha and Cui, 2002). This flow pattern is also observed in emergency core cooling of nuclear reactors, in oil extraction from wells, transportation in pipelines of hydrocarbons, and in geothermal and thermal power plants (Bugg et al., 1998; Fabre and Liné, 1992; Fernandes et al., 1983; Lu and Prosperetti, 2008; Mao and Dukler, 1991; Taha and Cui, 2006).

Gas bubbles are often used to promote mixing and mass transfer in several types of reactors (Bi, 1999; Braak et al., 2011; Campos and Carvalho, 1988b; Elperin and Fominykh, 1997), and slug flow has been described as an excellent alternative to mechanical induced agitation. Terrier et al. (2007) described a new bubble column disposable bioreactor, where Taylor bubbles promote mixing and aeration. According to the authors, the Slug Bubble Bioreactor allowed for an easy scale-up by using the desired number of multiple units, being compact, efficient, robust, easy to operate aseptically, flexible and cost effective.

Examples of slug flow are also observed on physiological and geological systems. At the capillaries, red blood cells behave similarly to Taylor bubbles due to the stress-induced deformation of their shape (Kang et al., 2010). In gas embolism, caused by the presence of gas bubbles within the cardiovascular system - a situation that can lead to a patient's death -, the bubbles are, in fact, Taylor bubbles. Slug flow is also a common phenomenon in volcanology, where large gas bubbles rise through basaltic magma during volcanic eruptions, often resulting in Strombolian eruptions,

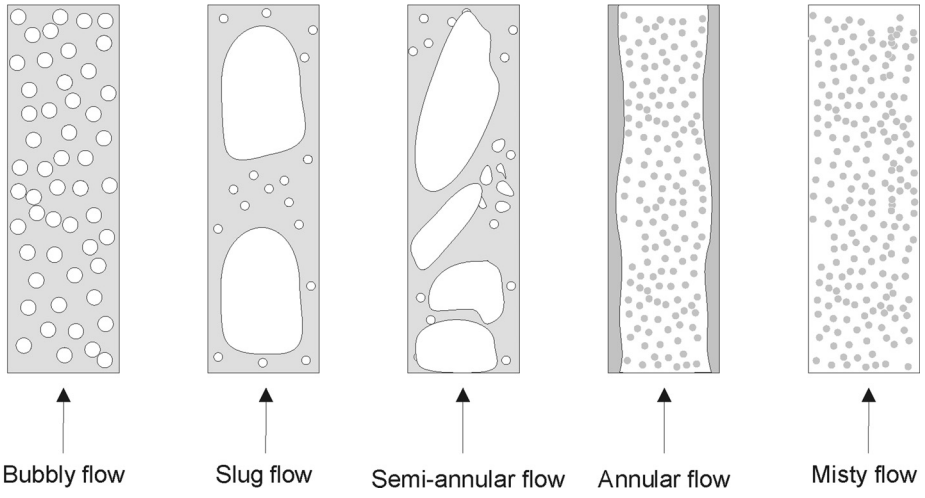

Fig. 1. Schematic representation of the different types of gas–liquid flow patterns commonly referred in the literature.

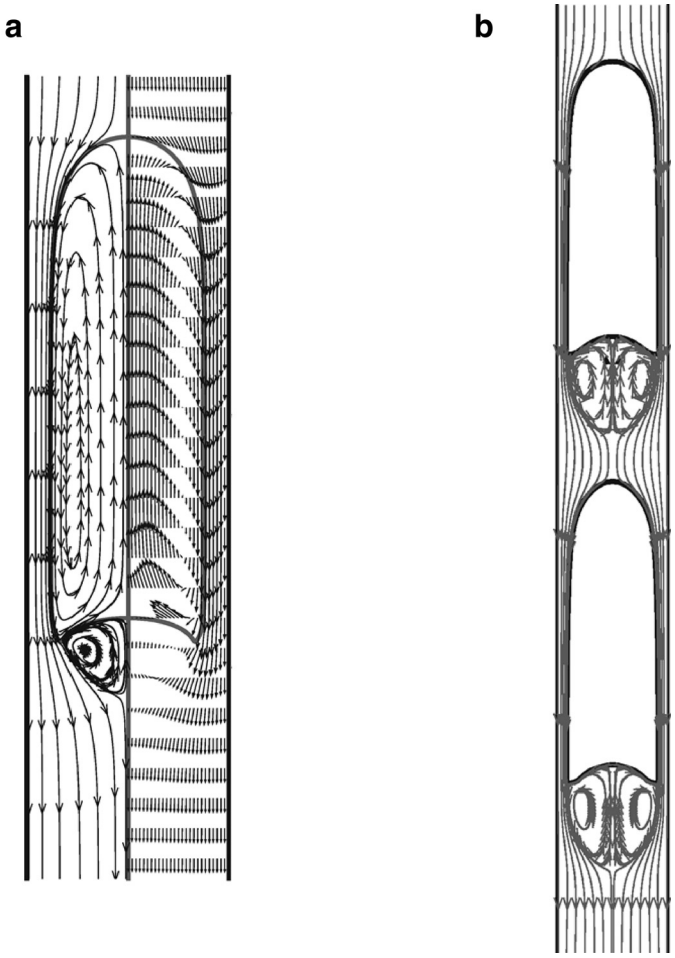

Fig. 2. Numerical images of the flow around (a) a single Taylor bubble and (b) two consecutive Taylor bubbles rising through stagnant liquid.

reported to be caused by the quasi-periodic formation, expansion and bursting of Taylor bubbles separated by magmatic slugs (James et al., 2011; Pering et al., 2015; Pino et al., 2011; Seyfried and Freundt, 2000).

The motion of large gas bubbles through liquids has been the focus of the scientific community since the 1940s, with the pioneer study of Dumitrescu (1943) on the motion of a single large gas bubble rising through stagnant liquid in a vertical tube. The early works of Davies and Taylor (1950), Laird and Chisholm (1956), White and Beardmore (1962), Nicklin et al. (1962), Brown (1965), Zukoski (1966), Wallis (1969), among others, shed significant light on the complex motion of Taylor bubbles. In the recent years, the development of non-intrusive optical experimental techniques, such as Particle Image Velocimetry and Pulsed Shadow Technique, contributed to further understand Taylor bubbles characteristics, hydrodynamic features on the surrounding liquid, and to the validation of theoretical models for the bubble velocity and of experimental data taken from photographic studies (Bugg and Saad, 2002; Polonsky et al., 1998, 1999a,b; van Hout et al., 2002b).

A myriad of other experimental studies on slug flow allowed for the gathering of a great amount of information on this flow pattern, being essential for understanding its hydrodynamics (Bendiksen, 1985; Campos and Carvalho, 1988a,b; DeJesus et al., 2012; Mao and Dukler, 1989; Nakoryakov et al., 1986, 1989; Nogueira et al., 2006a,b; Pinto et al., 1998, 2005; Shemer et al., 2007a,b). However, the complexity of slug flow, arising from its aperiodic behavior both in space and in time, often reveals the limitations of a pure experimental approach (Nogueira et al., 2003). Numerical studies have, thus, been of uttermost importance to overcome such difficulties, and complement experimental works (Araújo et al., 2012; Bugg et al., 1998; Clarke and Issa, 1997; Kang et al., 2010; Kawaji et al., 1997; Lu and Prosperetti, 2008; Taha and Cui, 2006; Tomiyama et al., 1996). Examples of the symbiotic association between experimental and simulation studies are the works of Tomiyama et al. (1996) and Mayor et al. (2008a, 2007a, 2008c, 2007b). The first authors used experimental data on the effects of Eötvös and Morton dimensionless groups on the shape of Taylor bubbles to assess the feasibility of numerical simulation of vertical slug flow using the volume-of-fluid (VOF) methodology, while Mayor et al. used empirical bubble-to-bubble interaction correlations relating the bubble velocity and the length separating consecutive Taylor bubbles, taken from an experimental analysis, as input in a Slug Flow Simulator, SFS. The SFS allows to assess, for the conditions tested, the influence of the inlet slug length distribution on the development of continuous slug flow, and also the extent of the column entrance length, in different scenarios: fully turbulent regime (in the near wake of the leading bubble and in the main liquid), fully laminar regime and a mixed scenario of laminar flow in the main liquid and turbulent one in the wake.

The importance of slug flow in practical applications has culminated in the great number of works published on the subject, and the need to systematize the data available in the literature

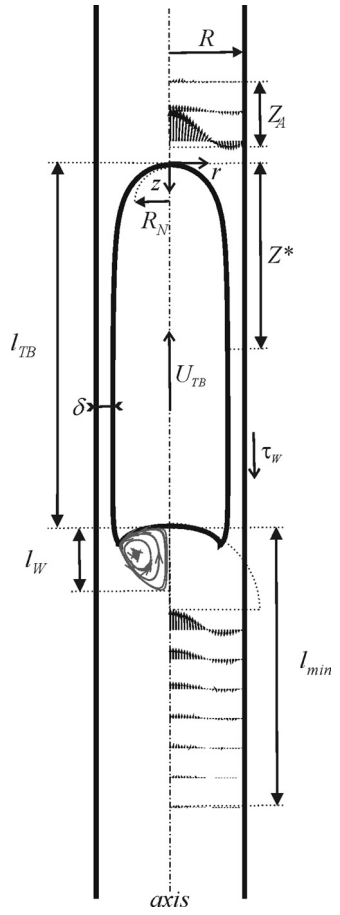

Fig. 3. Schematic representation of the main hydrodynamic features assessed in the present review.

constitutes the driving force for the present review on the hydrodynamics of Taylor bubbles rising in vertical tubes through both stagnant and co-current flowing liquids. In this work, the characteristic features of vertical gas–liquid slug flow are reviewed (for further information on liquid–liquid and three-phase systems see Mandal et al. (2007), Mandal et al. (2009), Hayashi et al. (2011), Hall (1997), Pavlidis et al. (2014)), starting with a dimensional analysis of the variables affecting the flow of an individual Taylor bubble. First, the velocity field and a description of the hydrodynamic features at the characteristic flow regions (near the nose, liquid film and wake) are assessed in the simplest case of a single Taylor bubble rising through stagnant liquid, and afterwards in the case of co-current flowing liquid. Furthermore, continuous slug flow and the interaction between consecutive Taylor bubbles are also addressed. A schematic representation of the main hydrodynamic features assessed can be observed in Fig. 3, including the bubble velocity (U_{TB}), the radius of curvature at the nose (R_N), the interaction distance above the bubble (Z_A), the length needed to have fully developed annular liquid film ($Z*$), the film thickness (δ), the wall shear stress in the stabilized film (τ_W), and the wake dimensions, represented by its length (l_W).

Although there are other published reviews on these subject, those date back to the early 90s (Fabre and Liné, 1992; Taitel and Barnea, 1990). As it will be described throughout this work, the significant development of new and improved experimental and numerical techniques that occurred in the last two and half decades allowed for a deeper understanding of the hydrodynamics of slug flow. As aforementioned, the need to systematize the large number of results arising from these new studies underpins the writing of the present review. It should be noted that in the *Encyclopedia of Two-Phase Heat Transfer and Flow* published by Thome (2015), Taitel and Barnea wrote a review on the modeling of gas-liquid flow in pipes. However, and as in Taitel and Barnea (1990), such review follows a clearly different approach from the one adopted in the present review. Taitel and Barnea's approach is based in Fernandes et al. (1983) model, which establishes macroscopic balances to the two phases and quantifies the various physical parameters comprising those equations, while here the different physical mechanisms inside the flow of a Taylor bubble are extensively assessed through dimensional analysis, following the work of White and Beardmore (1962). From the present authors point of view, both approaches are complementary: Fernandes et al. (1983) model is useful to any designer who needs to characterize two-phase flow, whereas the approach here adopted is preferable to someone who desires to understand the physical mechanisms associated with slug flow.

The present review is focused on gas-liquid slug flow on vertical tubes with a circular cross-section. Hence, the cases of inclined and horizontal columns, as well as columns with non-circular cross sections will not be assessed. These topics have been covered in the works of Dukler and Hubbard (1975), Cook and Behnia (2000), James et al. (2004), Van Hout et al. (2003), Wang et al. (2014b) and (2014a). Considering microfluidic systems, here too not addressed, the works of Angeli and Gavriilidis (2008), Gupta et al. (2010) and Zhao and Middelberg (2011) provide a detailed insight on the current state-of-the-art on this topic. Also outside the scope of this work are the numerical methods and experimental techniques employed in multiphase flow, subjects investigated by Cassidy et al. (2009), Hao and Prosperetti (2004), Talimi et al. (2012), Abdulkadir et al. (2015) and Do Amaral et al. (2013), among others.

2. Dimensional analysis

Throughout its rise in a vertical column of stagnant liquid, an individual Taylor bubble is influenced by gravitational, inertial, viscous and interfacial forces. White and Beardmore (1962) analyzed empirically the problem of the estimation of the bubble rising velocity (U_{TB}) using dimensional analysis through the Pi-Buckingham theorem. According to them, U_{TB} depends on: g, the acceleration due to gravity; D, the tube internal diameter; the physical properties of both the liquid (denoted by the index L) and the gas (index G), namely their density, ρ, viscosity, μ, as well as the gas-liquid surface tension, σ; and on the geometrical parameters describing the bubble, given by its length, l_{TB}. The same dependence was reported by Collins et al. (1978) and, more recently, by Hayashi et al. (2010, 2011) and Taha and Cui (2006), among others.

From dimensional analysis, and neglecting the effects of the expansion of the gas bubble during its rise, it follows that:

$$\frac{{U_{TB}}^2.\rho_L}{g.D.(\rho_L-\rho_G)} = f\left(\frac{g.(\rho_L-\rho_G).D^2}{\sigma}, \frac{g.\mu^4.(\rho_L-\rho_G)}{\rho_L^2.\sigma^3}, \frac{\rho_L}{\rho_G}, \frac{\mu_L}{\mu_G}, \frac{l_{TB}}{D}\right) \quad (1)$$

The previous equation is equivalent to say that the Froude number, given by:

$$\mathrm{Fr} = \frac{{U_{TB}}^2.\rho_L}{g.D.(\rho_L-\rho_G)}, \quad (2)$$

is a function of the aforementioned dimensionless groups, where $\frac{g.(\rho_L-\rho_G).D^2}{\sigma}$ is the Eötvös group (Eo), representing the ratio between surface tension and gravitational effects, and $\frac{g.\mu^4.(\rho_L-\rho_G)}{\rho_L^2.\sigma^3}$ the Morton group (M), also known as the property group, for

containing only the properties of the fluid. Thus, Eq. (1) can be rearranged as:

$$\mathrm{Fr} = f\left(\mathrm{Eo},\ \mathrm{M},\ \frac{\rho_L}{\rho_G},\ \frac{\mu_L}{\mu_G},\ \frac{l_{TB}}{D}\right) \tag{3}$$

For gas bubbles rising through a continuous liquid phase, the groups $(\rho_L - \rho_G)/\rho_L$ and μ_L/μ_G might be negligible since gases density and viscosity are generally much smaller than those of the liquids (Hayashi et al., 2010, 2011; Taha and Cui, 2006; White and Beardmore, 1962).

White and Beardmore (1962) also reported that bubble-shape factors might not be required to describe the motion of an individual Taylor bubble, owing primarily to two factors: (1) as previously stated, $\rho_L \gg \rho_G$, and thus the pressure along the bubble surface is constant, allowing it to hold its diameter along the axial direction; (2) the rise of a bubble is mostly affected by the flow field above its nose, hence its length is expected to have a significant impact only on the velocity profile of the liquid film flowing in the annular space between the tube wall and the bubble, which will be assessed ahead. For sufficient long bubbles, such as Taylor bubbles normally are, their length is sufficient to ensure a fully developed liquid film.

The previous considerations allow for the simplification of Eq. (3), and the following set of three dimensionless groups are sufficient for the characterization of the rise of a single Taylor bubble through a vertical column of stagnant liquid:

$$\mathrm{Fr} = f(\mathrm{Eo},\ \mathrm{M}). \tag{4}$$

In spite of the aforementioned, several dimensionless groups may arise by variable recombination. Besides the last set of dimensionless groups, Eq. (4), other commonly used in fluid mechanics could be chosen, such as Reynolds, *Re*, and Weber, We, groups: while performing a dimensional analysis of terminal velocity of Taylor bubbles and Taylor drops: Hayashi et al. (2010, 2011) suggested a correlation for Fr as a fundamental function of the bubble/drop Reynolds number and Eötvös group. Moreover, the Froude group can be described as a unique function of the Morton group and of the inverse viscosity number, N_f, a dimensionless group given by:

$$\mathrm{N}_f = \sqrt{\frac{\rho^2.g.D^3}{\mu^2}} = \frac{\sqrt{g.D^3}}{\upsilon} = \left(\frac{\mathrm{Eo}^3}{\mathrm{M}}\right)^{1/4}, \tag{5}$$

where υ represents the kinematic viscosity, $\upsilon = \mu/\rho$.

Wallis (1969), while studying one-dimensional two-phase flow, used Fr and N_f together with the Archimedes number:

$$\mathrm{Ar} = \frac{\sigma^{3/2}.\rho_L}{{\mu_L}^2.\sqrt{g.(\rho_L - \rho_G)}} \sim \frac{\sigma^{3/2}.{\rho_L}^{1/2}}{{\mu_L}^2.g^{1/2}} = \sqrt{\frac{1}{\mathrm{M}}}. \tag{6}$$

Fabre and Liné (1992) used Fr as a unique function of Eo and N_f, while Pinto et al. (1998) considered a function of N_f and M, adding that, for sufficiently large tubes and liquids with low viscosities, U_{TB} becomes independent of ρ_L, μ_L and σ, and so Fr becomes constant and independent of N_f and M, as it will be described in the next section. Furthermore, the Eötvös group is also related to a group used by Barr (1926), among others: the r/a group, with $a^2 = 2\sigma/\rho.g$ being the "specific cohesion". The relation between the groups can be expressed as:

$$\mathrm{Eo} = 8(r/a)^2. \tag{7}$$

White and Beardmore (1962) plotted a wide spectrum of experimental data on Taylor bubbles rising through vertical columns of motionless liquid, depicting regions in which the effect of some retarding forces becomes negligible (Fig. 6 of their work). As an example, they suggested that, when inertial forces have a minor effect on the bubble motion, the Poiseuille number:

$$\mathrm{Ps} = \frac{U_{TB}.\mu_L}{\rho_L.g.D^2}, \tag{8}$$

representing the ratio between viscous and gravitational forces, can substitute Fr as the group containing U_{TB}. The graphical findings of White and Beardmore (1962) will be addressed in the following section.

3. Taylor bubble velocity in stagnant liquid

The rise of a single Taylor bubble through stagnant liquid in a vertical tube was first studied by Dumitrescu (1943). In this theoretical study, the author proposed that such motion could be approximated by that of a bubble rising through an inviscid liquid, and, within this framework, the bubble velocity was determined under potential flow. Using a coordinate system fixed on the bubble, Dumitrescu first applied the conditions of conservation of vorticity to find an approximate solution by considering constant vorticity upstream the bubble. Afterwards, an approximate solution for potential flow around the nose - assuming it to be spherical - and an asymptotic solution for an inviscid falling film with a common tangent at the surface junction were matched, in order to find the integration constant. Doing so, Dumitrescu found the following expression for the velocity of a single Taylor bubble through stagnant liquid within a vertical tube, neglecting viscous and surface tension effects, as well as bubble expansion during the rise:

$$U_{TB} = 0.351\sqrt{g.D}. \tag{9}$$

A similar scenario, *i.e.*, isolated Taylor bubble rising in stagnant vertical columns of nitrobenzene and water, was studied by Davies and Taylor (1950). Experimentally, measurements of the shape of the bubble nose and its rising velocity were performed. The authors then analyzed the data theoretically, assuming the pressure over the front of the bubble to be the same as that in an ideal hydrodynamic flow around a sphere. Considering potential flow around the bubble, Davies and Taylor truncated the theoretical Bessel function series solution for the stream function retaining only the first term and, thus, following a less accurate method (Tung and Parlange, 1976), which gave rise to 0.328, a lower result when compared with the 0.351 value of Eq. (9).

It is particularly impressive the agreement between the solution from Dumitrescu (1943) and those found experimentally by White and Beardmore (1962), Nicklin et al. (1962) and Zukoski (1966), as well as in the numerical simulations of Mao and Dukler (1991).

As mentioned in the previous section, the bubble length is not a factor that influences the motion of an individual Taylor bubble. In fact, bubble velocity will depend on its length only for short bubbles, for which stabilization of the annular liquid film is not achieved. The validation of Eq. (9) through numerous experimental and numerical studies, despite not taking into account the bubble length, constitutes an additional support in favor of the minor impact of this parameter on U_{TB}.

The effect of the gas expansion on the bubble velocity as it rises towards lower pressure regions was recognized by White and Beardmore (1962). In this watershed work, the authors proposed a general graphical correlation for the rise velocity of single Taylor bubbles in vertical tubes, described by the dimensionless Froude, Morton and Eötvös numbers, as well as a graphical representation highlighting regions where the effects of some of the governing forces (gravitational, inertial, interfacial and viscous) can be neglected. Table 1 summarizes the limits of the correlation and the corresponding values considered by White and Beardmore (1962).

As it is possible to infer from the observation of Table 1, Eq. (9) applies only to the inertia-controlled regime, region VI. Analyzing the impact of surface tension in the velocity and shape of

Table 1
Ranges of predominance of the governing forces and corresponding correlations proposed by White and Beardmore (1962).

Region	U_{TB} independent of the effects of	Correlation	Correlation limits (approx.)			
			Fr	M	Eo	N_f
I	Inertial and viscous forces	$U_{TB} = 0$	–	–	< 4	–
II	None	Graphical	–	$10^{-12} - 10^{8}$	$3 - 400$	–
III	Viscous forces	Graphical	–	–	–	$> \sqrt{3 \times 10^5}$
IV	Interfacial forces	Graphical	–	–	> 70	–
V	Inertial forces	Graphical	< 0.05	–	–	–
VI	Viscous and interfacial forces	$U_{TB} = 0.345\sqrt{gD}$	–	–	> 70	$> \sqrt{3 \times 10^5}$

long bubbles rising through tubes, Bretherton (1961) pointed out the existence of a limiting Eo value bellow which bubbles will not rise, in agreement with the early findings of Hattori (1935) and Barr (1926). Bretherton (1961) suggested this value to be 3.37, while White and Beardmore (1962) adopted Eo ≤ 4 as the criterion for zero bubble velocity (region I from Table 1, corresponding to surface-tension controlled regime). However, different critical Eo values around these may be obtained, insofar as the contact angle between the liquid and the tube wall will depend on the cleanliness and roughness of the tube surface. The case of non-negligible viscous forces was initially studied by Goldsmith and Mason (1962), culminating in the deduction of a model for large bubble motion in low Reynolds regimes accounting for the bubble velocity's dependence on the liquid viscosity. Furthermore, the experimental and theoretical study of Brown (1965) on the effect of the liquid viscosity on U_{TB} showed that, although the potential flow solution describes well the bubble velocity for low viscosity liquids, it does not hold for highly viscous ones. Given so, Brown (1965) proposed a more general form for Eq. (9) including the effects of the liquid viscosity. This correlation can be found in Table 2, which contains a schematic compilation of the main correlations proposed for the rising velocity of a Taylor bubble through a stagnant liquid in a vertical tube. In spite of the aforementioned findings regarding the surface tension and viscosity controlled regimes, the inviscid fluid assumption is expected to be an accurate approximation for several practical cases of slug flow, according to Fabre and Liné (1992), who published, in the early 90s, an extensive review on two-phase slug flow modeling.

In the second half of the 60s, further insight was gained on the influence of all relevant variables on U_{TB}, namely through the works of Zukoski (1966) and of Wallis (1969). While the first consisted on an experimental study on the effects of liquid viscosity and density, surface tension, and tube diameter and inclination on the bubble velocity, the second proposed a general correlation for U_{TB} in terms of all those variables, for instance, it takes into account the limiting Eötvös number below which there is zero bubble velocity through the exponent $(3.37 - \mathrm{Eo})$ (see Table 2). Another correlation for the rise velocity of a single Taylor bubble in a vertical pipe containing stagnant liquid was proposed by Tung and Parlange (1976) who, by using large diameter tubes in order to supress viscous effects and isolate interfacial forces, found this velocity to decrease as surface tension increases. More recently, Viana et al. (2003) proposed a universal correlation to determine the rise velocity of long bubbles in round tubes based on experimental data gathered from literature, as well as from experiments performed by the authors (see Table 2). These authors processed the data in log-log Fr *vs.* *Re* plot for fixed ranges of Eo that yielded power laws in Eo for the higher and lower values of *Re*, with the transition region between those ranges being fitted by a logistic dose curve. Considering that the correlation of Viana et al. (2003) results from data processing only without a deeper understanding of the phenomena insights, Funada et al. (2005) theoretically derived an expression for the rise velocity of a Taylor bubble, modeled as an ovary ellipsoidal cap bubble, in a viscous, irrotational liquid. Applying viscous potential theory to the nose of the bubble, the authors derived an expression for the rise velocity as function of the inverse viscosity and the Eötvös numbers, as well as the nose shape, allowing its prediction from experimental velocity data. Doing so, Funada et al. (2005) reported the shape of the bubble nose to be strongly influenced by surface tension, since its dependence on Eo is much greater than on N_f.

To visualize their quality and applicability, the curves predicted by the correlations from Wallis (1969) and Viana et al. (2003) are depicted in Fig. 4 and compared with the experimental data from White and Beardmore (1962) and with the numerical results from Araújo et al. (2012). The agreement between numerical and experimental data is noticeable. Comparing the empirical correlations, a better fitting seems to be obtained prescribing the one from Viana et al. (2003), in agreement with the findings of Araújo et al. (2012). Also noteworthy is the separation of the data between the different Morton numbers, with bubble velocity decreasing for higher values of this dimensionless parameter (lower Fr values over the entire range of Eo). Such behavior is probably the result of the growing importance of the viscous forces on the bubble motion. Furthermore, it is visible an overlapping of the Fr *vs.* Eo curves for decreasing Morton number, suggesting the existence of a critical M value (in an order of magnitude of 10^{-8}) for which the bubble velocity becomes independent of the viscous effects. The maximum Froude number tends to the value of 0.35, as expected.

Hayashi et al. (2010) proposed an empirical correlation for the Taylor bubbles' terminal velocity in vertical pipes (see Table 2). These authors used dimensional analysis, based on the local instantaneous fields equations and on the jump conditions (Ishii, 1975), to obtained the correlation functional form, while its coefficients were determined by investigating the limiting cases of $(\mathrm{Eo} \to \infty, Re_{TB} \to \infty)$ and $(\mathrm{Eo} \to \infty, Re_{TB} \to 0)$ combined with an assessment of experimental data. Despite the good agreement between Hayashi's correlation and other correlations for the rising velocity of Taylor bubbles (Tung and Parlange, 1976; Viana et al., 2003; Wallis, 1969), Kurimoto et al. (2013) proposed an alteration of the coefficients values reported by Hayashi et al. (2010) (see Table 2). Such modification was due to an incoherence in the values quoted by Viana et al. (2003) from White and Beardmore (1962) data for low Morton number, which were used by Hayashi et al. (2010) to determine the Fr correlation coefficients. Furthermore, the consequences of the error detected by Kurimoto et al. (2013) are visible in Fig. 4, since the experimental and numerical data are best fitted by Wallis's correlation, for the curves corresponding to $\mathrm{M} < 10^{-2}$.

As aforementioned, the majority of the works on the motion of an individual Taylor bubble rising through a vertical column of stagnant liquid do not take into consideration the effects of bubble gas expansion. Gas expansion effectively occurs when the top end of the pipe is open to the atmosphere and the bubble rises through an incompressible liquid. Sousa et al. (2006) experimentally studied this effect on the velocity of a single

Table 2
Summary of the main correlations proposed in the literature for the rising velocity of a Taylor bubble in a vertical tube of stagnant liquid.

Author(s)	Type of study	Correlation	Assumptions and comments
Dumitrescu (1943)	Theoretical	$U_{TB} = 0.35\sqrt{gD}$	• Inviscid liquid • Constant upstream vorticity • Spherical nose • Negligible bubble expansion, viscous and surface tension effects • Potential flow
Davies and Taylor (1950)	Theoretical	$U_{TB} = 0.328\sqrt{gD}$	• Pressure over the bubble's nose equal to that over an ideal sphere • Negligible bubble expansion, viscous and surface tension effects • Potential flow
White and Beardmore (1962)	Experimental	$U_{TB} = 0.345\sqrt{gD}$ for inertia-controlled regime Graphical correlations for regimes controlled by different retarding forces	
Brown (1965)	Experimental and Theoretical	$U_{TB} = 0.35\sqrt{gD}\sqrt{1-2\left(\frac{\sqrt{1-ND}-1}{ND}\right)}$ $N = \sqrt[3]{14.5\rho_L^2 g/\mu_L{}^2}$	• Empirical application limits Surface tension: $\frac{\rho_L g D^2}{4\sigma}\left(1-2\left(\frac{\sqrt{1-ND}-1}{ND}\right)\right)^2 > 5.0$ Viscosity: $ND > 60$
Wallis (1969)	Theoretical	$\mathrm{Fr} = \frac{U_{TB}}{\sqrt{g.D}} = 0.345\left(1-e^{-0.01\mathrm{N}_f/0.345}\right)\left(1-e^{(3.37-\mathrm{Eo})/m}\right)$ $m = \begin{cases} 25, & \mathrm{N}_f < 18 \\ 69\mathrm{N}_f{}^{-0.35}, & 18 < \mathrm{N}_f < 250 \\ 10, & \mathrm{N}_f > 250 \end{cases}$	
Tung and Parlange (1976)	Experimental and Theoretical	$\mathrm{Fr} = \frac{U_{TB}}{\sqrt{gD}} = \sqrt{0.136 - 0.944\frac{\sigma}{\rho_L g D^2}}$	• Negligible viscous effects • Isolated interfacial effects • Excellent agreement with experimental data
Viana et al. (2003)	Experimental	$\mathrm{Fr} = \frac{U_{TB}}{\sqrt{g\ D}}$ $\mathrm{Fr} = \frac{0.34/(1+3805/\mathrm{Eo}^{3.06})^{0.58}}{(1+(\frac{\mathrm{R}}{31.08}(1+\frac{278.76}{\mathrm{Eo}^{1.96}})^{0.49})^{-1.45(1+\frac{7.22\times10^{13}}{\mathrm{Eo}^{9.93}})^{0.094}})^{0.71(1+\frac{7.22\times10^{13}}{\mathrm{Eo}^{9.93}})^{-0.094}}}$ $\mathrm{R} = \frac{\sqrt{D^3 g\rho_L(\rho_L-\rho_G)}}{\mu_L} \sim \mathrm{N}_f$	
Hayashi et al. (2010)	Experimental and Numerical	$\mathrm{Fr} = \frac{U_{TB}}{\sqrt{gD}} = \sqrt{\frac{0.0089}{0.0725+\frac{1}{\mathrm{Re_{TB}}}(1-0.11\mathrm{Re_{TB}}^{0.33})}\left(1+\frac{41}{\mathrm{Eo}^{1.96}}\right)^{-4.63}}$	• $10^{-7} < \mathrm{Re_{TB}} < 10^4$ • $4 < \mathrm{Eo} < 3\times10^3$ • $10^{-2} < \mathrm{N}_f < 10^5$ • $10^{-11} < \mathrm{M} < 10^{10}$
Kurimoto et al. (2013)	Experimental and Numerical	$\mathrm{Fr} = \frac{U_{TB}}{\sqrt{gD}} = \sqrt{\frac{G.H}{\frac{H}{0.35^2}+F}}$ $G = \left(1+\frac{3.87}{\mathrm{Eo}^{1.68}}\right)^{-18.4}$ $H = 0.0025[3+G]$ $F = \frac{1}{\mathrm{Re_{TB}}}(1-0.05\sqrt{\mathrm{Re_{TB}}})$	

Taylor bubble rising in stagnant conditions. Despite having used solutions of carboxymethylcellulose polymer (0.01–0.1 wt%), a non-Newtonian fluid, the authors reported that, as a result from the very low velocity gradients in the flow field ahead of the bubble nose, the maximum shear rate was closed to $1\,s^{-1}$, and thus, in that region, the solutions had a Newtonian behavior with almost uniform viscosity. Being so, Sousa et al. (2006) found that gas expansion leads to an increase in the bubble velocity, which is length dependent. However, since the velocity ahead of the bubble nose also increases with the increase in the bubble length due to expansion, gas expansion effects on bubble velocity can be corrected by subtracting the maximum liquid velocity, occurring at the tube axis, to the experimental values of U_{TB}, yielding a constant bubble velocity, corresponding to that of a bubble rising in a tube closed at both ends.

4. Detailed hydrodynamics

4.1. Nose region

During its movement, the Taylor bubble displaces the liquid ahead of it, changing the velocity field at its front. In a frame of reference attached to the bubble, *i.e.*, moving with it (see Fig. 5), and far above from its nose, the undisturbed liquid flows downwards, at a uniform velocity equal to U_{TB}, with the radial component of the liquid velocity being zero. Approaching the bubble nose, the axial liquid velocity decreases, whereas the radial component increasingly develops due to the liquid displacement. At the tip of the bubble nose, however, commonly considered the origin of the $z\,vs.\,r$ axis, both the axial and radial liquid velocity components are zero, in which is often referred to as stagnation point.

Studies on the motion of Taylor bubbles have shed significant light on both the interface shape and flow around the nose region (Brown, 1965; Collins et al., 1978; Davies and Taylor, 1950; Dumitrescu, 1943; Funada et al., 2005; Joseph, 2003; Nickens and Yannitell, 1987). In recent years, development of non-intrusive optical experimental techniques, namely Particle Image Velocimetry (PIV), contributed to further understanding the hydrodynamic features regarding this particular flow region. In fact, applying PIV allowed several authors to obtain experimental data on the distance above the bubble, Z_A, where the impact of the rising bubble is felt (Bugg and Saad, 2002; Nogueira et al., 2006a, 2003; Polonsky et al., 1999a,b; Shemer, 2003; van Hout et al., 2002b). The most important results of some of those studies are summarized in Table 3.

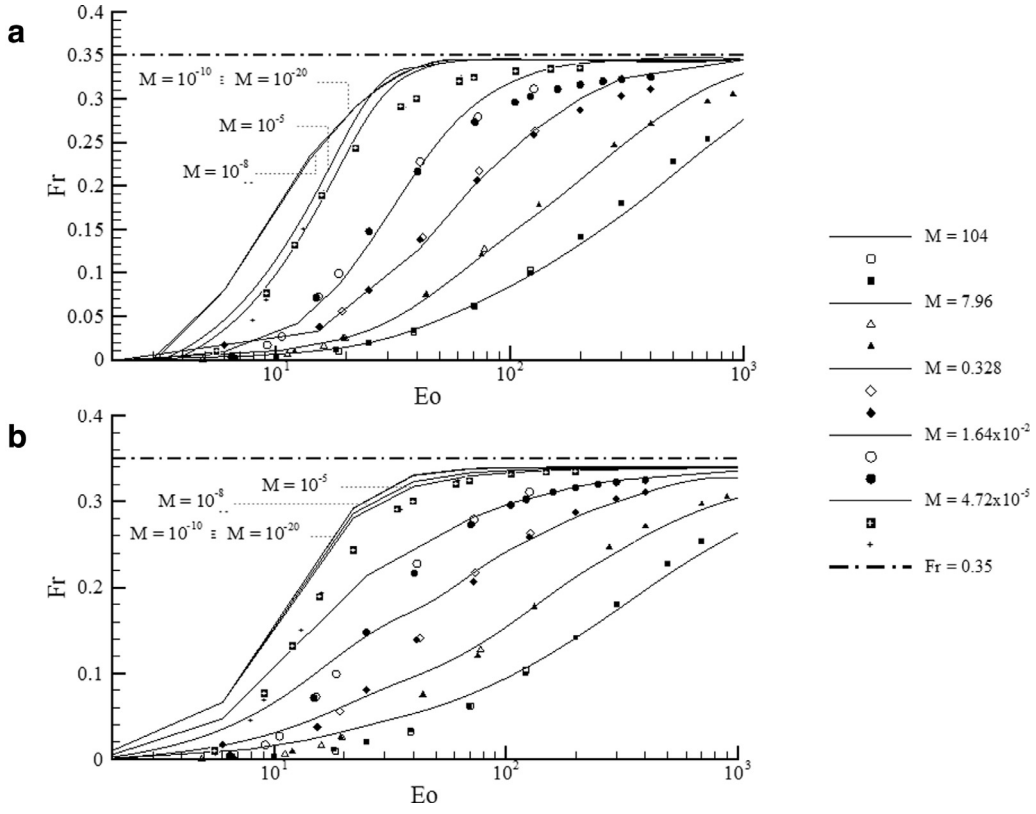

Fig. 4. Velocity of a Taylor bubble in a vertical column of stagnant liquid, $Fr = U_{TB}/\sqrt{gD}$, for a set of different Morton and Eötvös numbers. Comparison between the numerical results from Araújo et al. (2012) (closed symbols), the experimental data from White and Beardmore (1962) (opened symbols) and the curves predicted by the correlations of (a) Wallis (1969) and (b) Viana et al. (2003).

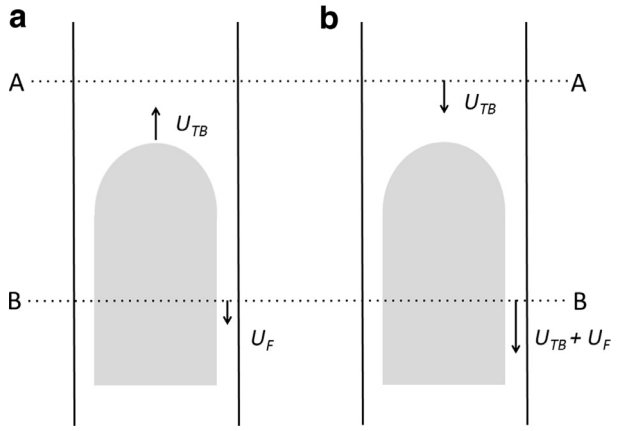

Fig. 5. Velocity patterns at planes A-A and B-B, in (a) a fixed frame of reference and in (b) a frame of reference moving with the Taylor bubble, for stagnant liquid.

The dimensionless interaction distance above the nose of a Taylor bubble, Z_A/D, was also assessed by Araújo et al. (2012), using a Computational Fluid Dynamics (CFD) commercial package that applied VOF as the interface capturing technique. Simulating the flow of single Taylor bubbles, in laminar regime, rising through stagnant Newtonian liquids, the authors reported that, for Morton numbers between 1.64×10^{-2} and 104, and $N_f > 40$, Z_A/D can be reasonably well-described by:

$$\frac{Z_A}{D} = 2.460 \times 10^{-2} \ln\left(N_f\right) + 0.393. \quad (10)$$

In this range of N_f, the authors observed little influence of the Morton number on Z_A/D, excepted for $M = 4.72 \times 10^{-5}$, value for which Z_A/D *vs.* N_f data started to deviate from Eq. (10). For $N_f < 40$, however, Z_A/D is approximately 0.483 and almost independent of M and N_f.

As previously mentioned, the shape of the bubble is an important feature to be assessed while studying the motion of Taylor bubbles. Dumitrescu (1943) was one of the firsts to study experimentally, through photographs, and theoretically, applying the potential flow theory, the shape of a Taylor bubble rising trough stagnant water contained in a vertical tube. Considering the origin of the axis to be located at the bubble nose, the author suggested that the bubble shape in the nose and the film regions could be

Table 3
Summary of data published in the literature for the dimensionless interaction distance above the nose of a Taylor bubble rising in a vertical tube containing stagnant liquid, Z_A/D.

Author	Polonsky et al. (1999b)	van Hout et al. (2002b)	Bugg and Saad (2002)	Shemer (2003)	Nogueira (2005)
Type of study	Experimental	Experimental	Experimental/Numerical	Experimental	Experimental
Technique	PIV	PIV	PIV/VOF	PIV	PIV-PST
Fluids	Air–water	Air–water	Air-olive oil	Air–water	Air-aqueous glycerol solutions
Regime	Turbulent	$Re_{TB} = 4350$	$Re_{TB} = 27$	Turbulent	Laminar
Z_A/D	0.66	0.55	0.30	0.50	0.57

described by:

$$\dot{x} = \begin{cases} 0.75\left(1 - \sqrt{1 - 1.778\dot{r}^2}\right), & \dot{x} \leq 0.5 \\ \dfrac{0.123}{\left(1 - \dot{r}^2\right)^2}, & \dot{x} \geq 0.5 \end{cases} \quad (11)$$

where $\dot{x}$ is the axial distance pointing downwards and normalized by the tube radius, R, and $\dot{r}$ is the distance from the tube centre line also normalised by R. It should be noticed that, despite Eq. (11) being in agreement with the experimental findings of Mao and Dukler (1991) for air-water systems, and with those of Nogueira et al. (2006a) for low viscosity solutions, it is only valid for inertia-controlled regime.

Focusing more specifically in the bubble interface along the nose region, experimental studies have reported interesting data. Nicklin et al. (1962), assessing two-phase slug flow in vertical columns of stagnant and co-current flow of liquid, suggested that the oblate spheroidal front of a Taylor bubble was only dependent of the flow conditions ahead of it, namely the liquid velocity field and viscosity. In fact, in the laminar regime, the curvature of the bubble nose has been reported to decrease for increasing liquid viscosities, as well as for increasing velocities of the Taylor bubble (Nogueira, 2005).

The curvature radius at the nose of a Taylor bubble, R_N, has been chosen by some authors as the parameter used to characterize the bubble shape in this region. Brown (1965) proposed an universal correlation for R_N as a function of the maximum radius of the Taylor bubble, R_{TB}:

$$R_N = 0.75R_{TB} = 0.75(R - \delta), \quad (12)$$

The experimental data from Bugg et al. (1998) and Nogueira et al. (2006a), as well as the numerical results reported by Mao and Dukler (1991), Taha and Cui (2006), Kang et al. (2010) and Araújo et al. (2012) suggest an increase in R_N with increasing values of the bubble velocity, and consequently Froude number, as well as with the inverse viscosity number.

4.2. Film region

The liquid displaced by the rise of a Taylor bubble flows downward as a thin film through the annular space between the bubble and the tube wall. Owing to flow continuity, as the radius of the cross-section of the bubble increases further from the nose, so does the average liquid velocity at the corresponding axial isosurfaces. Since the pressure adjacent to the film is constant - a consequence of the constant pressure at the interior of the gas bubble -, the gravitational forces acting on the liquid film must be balanced by both the shear stress at the wall and at the gas-liquid interface, and, thus, unlike the flow at the bubble nose (Nicklin et al., 1962), the flow in the film region depends on the bubble length.

As it flows further below the nose, the film boundary layer, initially adjacent to the tube wall, starts to develop, growing to occupy the entire annular region up to the gas-liquid interface (Fig. 6). As a consequence, the impact of viscous effects on the liquid film velocity profiles increases. As represented in Fig. 6, at a distance z from the nose where the film is fully developed, henceforth $Z*$, the thickness of the boundary layer is maximum, δ, and the bubble shape stabilises as a cylinder with a radius of $(R - \delta)$. For $z \geq Z*$, both the bubble shape and the velocity in the film are constant and independent of z. Supported by the tube wall, the annular liquid film acts as a free falling film flowing in a wetted wall column, ensuring that the assumption of unidirectional flow is acceptable (Campos and Carvalho, 1988a; Fernandes et al., 1983).

4.2.1. Velocity profile and film thickness

Several authors proposed correlations for the velocity profile in the fully developed annular liquid film and for the respective thickness, the most relevant of which are summarized in Table 4. Particular attention is given to the work of Brown (1965), as a great amount of experimental and numerical data published afterwards are in agreement with the results predicted by this author's equations.

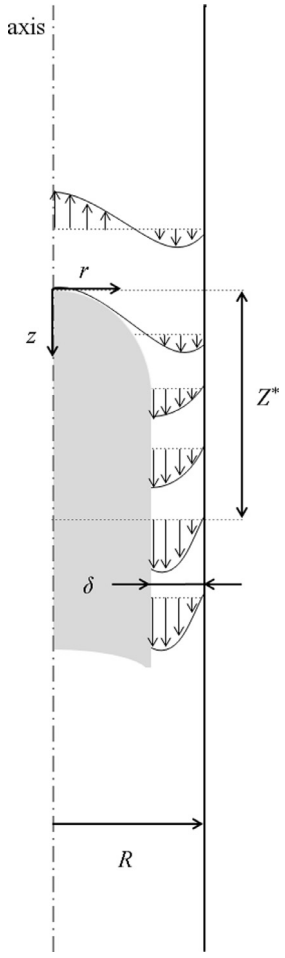

Fig. 6. Schematic representation of the development of the liquid film established between the Taylor bubble and the wall of the tube.

Brown (1965) proposed an alternative model to the inviscid liquid, taking into account the effect of the liquid viscosity in the film flow. Based on a frame of reference attached to the bubble, the author suggested that the liquid, approaching the bubble nose in true plug flow, suffers a deformation of its velocity distribution once it reaches the nose due to the pressure field at the stagnation point. Furthermore, Brown's model assumed the laminar layer of liquid to be fully developed near the bubble bottom, where it would be entirely supported by shear stress. Performing a balance in terms of gravity and shear stress forces on an infinitesimal cylindrical film element, the author obtained the equation shown in Table 4 for the velocity profile in the liquid film. The same expression was derived by Goldsmith and Mason (1962) while studying the motion of bubbles in inviscid fluids. Rearrangement of this liquid axial velocity equation, gives the expression for the thickness of the fully developed laminar film presented in the same table.

An analysis of the dependence of the annular film thickness on the inverse viscosity number was done, gathering δ data published by several authors. Processing the data assembled in the chart of Fig. 7, two regions are observed. For $N_f < 100$, the liquid film thickness is strongly influenced by the Morton number, *i.e.*, it presents a maximum and, then, decreases as N_f values

Table 4
Summary of the main correlations proposed in the literature for the velocity profile and the thickness of the fully developed annular film surrounding a Taylor bubble rising in a vertical tube containing stagnant liquid.

Author(s)	Velocity profile	Thickness of the annular film	Correlation limits	Assumptions and comments
Brötz (1954)	$U_F = \sqrt{196.7g\delta}$	$\delta(\frac{g}{\upsilon_L^2})^{1/3} = (\frac{3\mathrm{Re}_F^2}{\upsilon_L^2})^{1/3}$	$100 < \mathrm{Re}_F = \delta.U_F/\upsilon_L < 4,300$	• Study on the films of water and other fluids in turbulent flow regime, inside vertical tubes of various diameters
Brown (1965)	$U_F(r) = \frac{g}{\upsilon_L}(\frac{R^2-r^2}{4} - \frac{(R-\delta)^2}{2}\ln\frac{R}{r})$	$\delta = [\frac{3\upsilon_L U_{TB}}{2g}(R-\delta)]^{1/3}$	–	• Laminar regime in the film
Kay and Nedderman (1985)	$U_F(r) = \frac{g}{\upsilon_L}(\delta r - \frac{r^2}{2})$ At the interface, $r = \delta$, hence: $U_F = U_{F,\,max} = \frac{g\delta^2}{2\upsilon_L}$	–	–	• Liquid flowing down a vertical plane wall • Laminar and Newtonian fluid • $\delta \ll R$

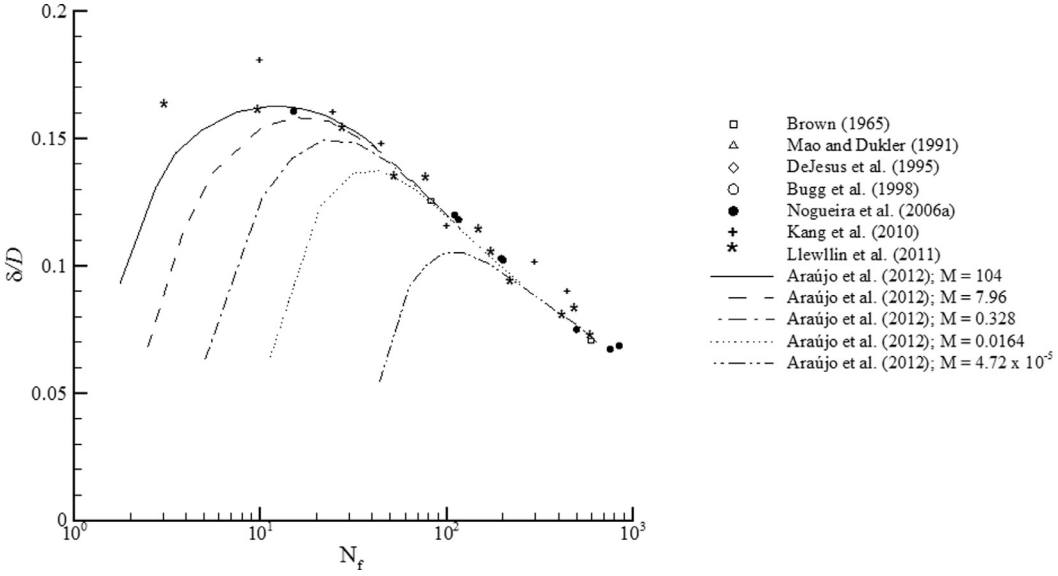

Fig. 7. Variation of the dimensionless developed liquid film thickness, δ/D, with the inverse viscosity number, $\mathbf{N_f}$.

increase, as reported by Araújo et al. (2012). For the set of M values addressed in their work (104, 7.96, 0.328, 0.0164 and 4.72×10^{-5}), the maximum value of the dimensionless thickness is higher for higher Morton numbers. Nevertheless, for values of the inverse viscosity number above 100, the liquid film thickness becomes independent of M, with the entire range of data assembled overlapping in a unique curve, which decreases as N_f increases. For $N_f > 100$, it should be also emphasized the agreement between the experimental (Brown, 1965; DeJesus et al., 2012; Llewellin et al., 2012; Nogueira et al., 2006a) and numerical (Araújo et al., 2012; Bugg et al., 1998; Kang et al., 2010; Mao and Dukler, 1991) data gathered . The deviation from Kang et al. (2010) and Llewellin et al. (2012) data for the lower N_f value is the result of the higher Morton number considered in these works, respectively 837 and 2560.

4.2.2. Stabilization length

In their studies on the liquid flow in the annular region between the tube and the bubble interface, Nicklin et al. (1962) and Batchelor (1967) reported the existence of a stabilized film (constant velocity and thickness) at a certain distance below the bubble nose. At a short distance down from the nose, both authors found that the viscous effects to be mostly negligible, except in a thin layer adjacent to the tube wall. Applying Bernoulli's equation along the free streamline, Nicklin et al. (1962) found the velocity in the liquid film relative to the nose to be given by $U_F = \sqrt{2gz}$. Considering the axial axis to point downwards with its origin at the tip of the bubble nose, z represents the distance from the nose. For increasing z values, the boundary layer at the wall grows to occupy the entire annular region between the tube and the surface of the bubble, with the influence of the viscous forces surpassing that of the gravitational ones. As the film velocity profile and the thickness become independent of z, the velocity along the free streamline, considering a reference attached to the Taylor bubble, will be given by:

$$U_F = U_{TB} + g\delta^2/(2\upsilon_L). \tag{13}$$

An estimate of the distance z from the nose where the film is fully developed, *i.e.*, at which the boundary layer reaches the free streamline, $z = Z^*$, can be obtained matching U_F from Bernoulli's equation and Eq. (13):

$$\sqrt{2gZ^*} = U_{TB} + g\delta^2/(2\upsilon_L) \Leftrightarrow Z^* = \frac{\left[U_{TB} + gd^2/(2\upsilon_L)\right]^2}{2g}. \tag{14}$$

4.2.3. Wall shear stress

The shear stress in the fully developed film around a Taylor bubble is given by:

$$\tau = \mu_L \frac{du_z}{dr}. \tag{15}$$

Deriving Brown (1965) equation for the axial velocity in the film along the radial direction of the tube, r, yields the following expression for the velocity gradient:

$$\frac{du_z}{dr} = \frac{g}{\upsilon_L}\left(\frac{r}{2} - \frac{(R-\delta)^2}{2r}\right). \tag{16}$$

Substituting Eq. (16) into (15) and applying it to the radial coordinate R, gives an expression for the wall shear stress (τ_w):

$$\tau_w = \rho_L . g \frac{\delta(2R-\delta)}{2R}, \tag{17}$$

which is equivalent to consider that, in the absence of friction at the free surface between the gas and the film, the wall shear stress supports the total weight of the liquid in the annular region.

In the literature, scarce data is found on the wall shear stress in the annular film, owing primarily to the inherent difficulties in preforming experimental measurements in this flow region. Numerical studies, however, have allowed for a growing understanding of the evolution of this parameter during the development of the liquid film (Araújo et al., 2012; Kang et al., 2010). Near the nose, the wall shear stress starts to increase. As a result of the development of the liquid film, a plateau is attained further down from the tip of the bubble. Near the bubble trailing edge, a steep decrease of τ_w usually occurs caused by the widening of the separation between the tube wall and the bubble interface. It should be noticed, however, that, for low values of Eo, the inflection in the standard shape of the bubble rear induces a peak in τ_w to occur immediately below the developed film (Araújo et al., 2012).

4.2.4. Laminar-turbulent transition

As the velocity of the liquid flowing downwards in the annular region between the tube and the surface of the Taylor bubble increases, transition from laminar to turbulent regime in the film may occur. The high degree of complexity inherent to the transition between flow regimes results in the scattered amount of lower and upper critical values found in literature to enclose the transition region in the liquid film flow (Fulford, 1964).

In order to study this transitional region, it is convenient to define a Reynolds number in the liquid film, Re_F. This can be done under the assumption of unidirectional flow in a liquid film on a vertical plate with a free surface, which is an acceptable approximation for the flow in the annular liquid film as previously explained. The Reynolds number for liquid flowing in a wetted wall column is given by:

$$Re_F = \frac{U_F . \rho_L . \delta}{\mu_L}. \tag{18}$$

From a frame of reference attached to the Taylor bubble rising through quiescent liquid, the bubble is stationary while the liquid is flowing downwards. At the cross-section defined by the plane A-A, in Fig. 5, the velocity of the liquid, U_L, must be equal in magnitude to the terminal rise velocity of the Taylor bubble, U_{TB}. On the other hand, at plane B-B, U_L must be higher than U_{TB} due to mass conservation: $U_L = U_{TB} + U_F$. The liquid flow rate entering cross-section A-A leaves through the B-B plane, yielding the following expression for the velocity in the liquid film:

$$U_F = \frac{U_{TB}}{\left(1 - \frac{(R-\delta)^2}{R^2}\right)} - U_{TB}. \tag{19}$$

Substituting Eq. (19) in Eq. (18), and considering the thickness of the developed annular film to be given by Brown's correlation (see Table 4), the Reynolds number of the liquid annular film can be alternatively written as:

$$\mathrm{Re}_F = \frac{U_{TB}}{\upsilon_L}\left[\frac{1}{1 - \frac{(R-\delta)^2}{R^2}} - 1\right]\left[\frac{3\upsilon_L U_{TB}}{2g}(R-\delta)\right]^{1/3}. \tag{20}$$

When $\delta \ll R$, Eq. (20) can be further simplified and Re_F written as:

$$\mathrm{Re}_F = \frac{U_{TB}}{\upsilon_L}\left[\frac{R}{2} - \left(\frac{3\upsilon_L R U_{TB}}{2g}\right)^{1/3}\right]. \tag{21}$$

Fulford (1964) published a review on the flow of thin films reporting Re_F data from several other authors. In thin films, a considerable portion of the thickness is still occupied by what is commonly called a "laminar sub-layer" and, thus, clearly marked boundaries for the transitional region are difficult to obtain. In spite of this, the majority of the results reported by Fulford (1964) allow for the establishment of indicative lower and upper critical Reynolds numbers for the transitional region, $[250; 400] < Re_F < 800$, being the lower limit less well defined than the upper one.

4.2.5. Turbulent regime

Turbulence is characterized by great flow complexity. Such intricacy is, once more, well reflected on the limited available data on turbulent fully developed flow in the liquid film. The assumption underpinning the most common treatment for turbulent liquid film flow is that a dimensionless profile valid for single-phase flow (pipe-flow) can be applied, being the form of this velocity profile what sets different methods apart. Studying the flow around a single Taylor bubble rising through stagnant and co-current flowing liquids, Nogueira (2005) followed the von Karman (1939) approach, which constitutes the base for the subsequent description made in the present work.

Considering a single-phase turbulent flow in a smooth pipe, and neglecting free surface oscillations, von Karman (1939) suggested the existence of an universal velocity profile valid for such conditions. This hypothesis was experimentally verified by Nikuradse (1933), who also demonstrated the existence of a buffer zone between the "laminar sub-layer" and the turbulent zone. In fact, as the velocity of the liquid flowing downwards in the annular region between the tube and the Taylor bubble surface increases and the flow regime changes from laminar to turbulent, three regions developed within the annular region: a laminar sub-layer close to the wall, a turbulent region near the gas–liquid interface, and, in between, a buffer layer.

Dukler and Bergelin (1952) used the resulting equations from von Karman (1939) approach, and, besides presenting the following limits of integration, which were suggested by Nikuradse data:

$$\begin{aligned} &\dot{u} = \dot{r}, \text{laminar sub} - \text{layer}, \dot{r} < 5 \\ &\dot{u} = -3.05 + 5.0 \ln \dot{r}, \text{buffer layer}, 5 < \dot{r} < 30, \\ &\dot{u} = 5.5 + 2.5 \ln \dot{r}, \text{turbulent zone}, 30 < \dot{r} < \dot{b}, \end{aligned} \tag{22}$$

arrived to the following expression for Re_F, upon integration of the dimensionless velocities over the entire film thickness for turbulent flow:

$$Re_F = \dot{b}\left(3.0 + 2.5 \ln \dot{b}\right) - 64. \tag{23}$$

In the above expressions, $\dot{u} = u/u^*$, u is the axial velocity, $\dot{r} = ru^*/\upsilon$, r is the distance from the wall, $\dot{b} = \delta u^*/\upsilon$ the dimensionless film thickness, and $u^* = \sqrt{\tau_w/\rho}$ is the friction velocity.

Careful observation of the limits of Dukler and Bergelin (1952) leads to an interesting finding: according to those authors, the film becomes turbulent for $\dot{b} = 30$, which, after substitution in Eq. (23), corresponds to $Re_F = 270$, falling within Fulford (1964) predictions for transitional flow.

Portalski (1963) compared the results for the experimentally measured film thickness of 13 liquids with the values predicted by the theories of Kapitsa (1949), Nusselt (1916), and the application of von Karman (1939) postulate, and reported the universal velocity profile concept to be the best available description of the turbulent film, predicting the average film thickness in fair agreement with experimental data.

4.3. Wake region

The importance of understanding the hydrodynamic characteristics of a Taylor bubble wake has been reported by several

authors. This region has significant influence in the interaction and coalescence of consecutive Taylor bubbles, and plays an important role in practical applications (Araújo et al., 2013a; Campos and Carvalho, 1988a,b; Nogueira et al., 2006b, 2003; Taha and Cui, 2006).

Although Moissis and Griffith (1962) reported that, in slug flow, the dynamics of a trailing Taylor bubble are affected by the flow pattern below the leading one, it was Maxworthy (1967) who showed the existence of well-defined wakes behind the bubbles. The simple visualization technique used by this author was later applied by Campos and Carvalho (1988a) in what is consider the first systematic study of the flow in the wake of individual Taylor bubbles rising through stagnant liquids.

Campos and Carvalho (1988a) photographic study constituted a watershed moment in the research of this region hydrodynamics. Considering the flow pattern in the wake to depend on D, ρ_L and μ_L, σ, l_{TB} and g, the authors reported the dimensionless wake volume, V_w/D^3, and length, l_w/D, to be a function of l_{TB}/D (where l_{TB} is the bubble length), Eo and N_f. Nevertheless, since the dependence on Eo is negligible for large-bore tubes ($D > 20$ mm), as it is the dependence on l_{TB}/D for sufficient large bubbles, Campos and Carvalho (1988a) suggested that the wake flow pattern is determined by N_f. In order to validate such hypothesis, experiments using aqueous glycerol solutions were performed, with viscosities ranging from 10^{-3} to 10^{-1} Pa s. The results showed a linear dependence of V_w/D^3 and l_w/D with N_f for $N_f < 800$. Additionally, three flow patterns were identified in the bubble wake over the entire range of N_f values:

Type I – Laminar wake, $N_f < 500$

Closed and axisymmetric wakes were observed, rising at the same velocity as that of the bubble. Inside the wake, the flow was laminar, with a vortex ring being found in a plane perpendicularly to the tube axis. The rear of the bubbles was shaped as an oblate spheroid with no oscillations occurring. Campos and Carvalho (1988a) proposed the following correlations for the dimensionless length and volume of the wake in this regime:

$$\frac{l_w}{D} = 0.30 \; + \; 1.22 \times 10^{-3} N_f, \tag{24}$$

$$\frac{V_w}{D^3} = 7.5 \times 10^{-4} N_f. \tag{25}$$

Type II – Transitional wake, $500 < N_f < 1500$

The wake was still closed, but lacking in symmetry. Vortex shedding occurred and periodic undulations of the vortex ring were observed. As a result of such undulations, whose frequency increases with N_f, the liquid flow around the bubble is unsteady and unaxisymmetric. Despite the difficulty in presenting a correlation for the dimensionless wake length and volume for such conditions, Campos and Carvalho (1988a) reported the wake length to increase with N_f.

Type III – Turbulent wake, $N_f > 1500$

For high N_f values, the wake opens and a turbulent flow is visible (see Fig. 8). The wake boundary is not well defined since viscous forces are no longer sufficient to stabilize the interaction between the falling film and the liquid rising in the wake, resulting in the development of turbulent eddies, whose action is felt at a distance of several diameters below the bubble rear. As in Type II, the quantification of the wake dimensions through visualization was difficult due to lack of boundary definition.

Quantification of l_w can be essential in practical slug flow applications such as air lift contactors or gas fluidized beds, where mixing is promoted by liquid displacement in the vicinity of the rising bubbles. Conducting experiments on the rise of Taylor bubbles in narrow columns of water, Campos and Carvalho (1988b) observed turbulent liquid flow in the bubble wake, contrasting with the orderly one around the nose and between the bubble and the tube wall. Under the assumption that the mixing induced by a rising slug is due solely to the liquid flow in a perfectly mixed wake, the authors proposed a simple model of mixing requiring only one parameter: the wake's length. Despite being based on a oversimplified assumption, the "fully mixed wake" model of Campos and Carvalho (1988b) has the distinct advantage of allowing to estimate with fair accuracy the extent of mixing induced by the motion of a given number of equal-sized Taylor bubbles rising through a narrow column of water.

Fig. 8. Long exposure photograph of a Taylor bubble rising through stagnant liquid. The paths of the small bubbles inside the liquid slug turbulent wake are visible.

Recent advancements in visualization techniques allowed for quantitative measurements of the flow fields in the wake of Taylor bubbles. Polonsky et al. (1999a) used PIV to study the oscillatory motion of the trailing edge of a Taylor bubble rising through stagnant and co-current water, having found that its amplitude depends on the liquid flow rate and on the bubble length, whereas its frequency is almost constant. Despite allowing the determination of velocity vectors near the gas–liquid interface, PIV fails to define its exact position and, thus, the shape of the bubble. Nogueira et al. (2003) combined PIV and Pulsed Shadow Technique, PST, techniques in order to overcome this downfall. These authors latter applied the same combined techniques to the experimental study of the flow around individual Taylor bubble rising through stagnant liquids and co-current Newtonian flows (Nogueira, 2005; Nogueira et al., 2006b). While the PIV technique allowed for the description of the wake flow pattern by means of instantaneous and average flow fields and corresponding streamlines, the shape of the bubble bottom was obtained from the PST. In spite of the high precision of this method on defining the boundaries of laminar wakes, optical distortion was identified when assessing the portion of the wake inside the concave bottom of the Taylor bubbles, and so quantification of the length and volume of the wakes for such cases did not take into account that inaccessible portion (Nogueira et al., 2006b, 2003).

Phase diagrams of the existence and type of wake, and of the shape of the Taylor bubble bottom were built based on data reported in literature (Fig. 9 and Fig. 10). The experimental (Shemer et al., 2007b; van Hout et al., 2002b) and numerical (Araújo et al., 2012; Kang et al., 2010; Lu and Prosperetti, 2008; Taha and Cui, 2006) data assembled were compared with the curves (thicker lines in both figures) suggested by Araújo et al. (2012) for the wake formation, Fig. 9, and for the transition in the shape of the bubble rear, Fig. 10. Furthermore, in Fig. 9, the data gathered for the

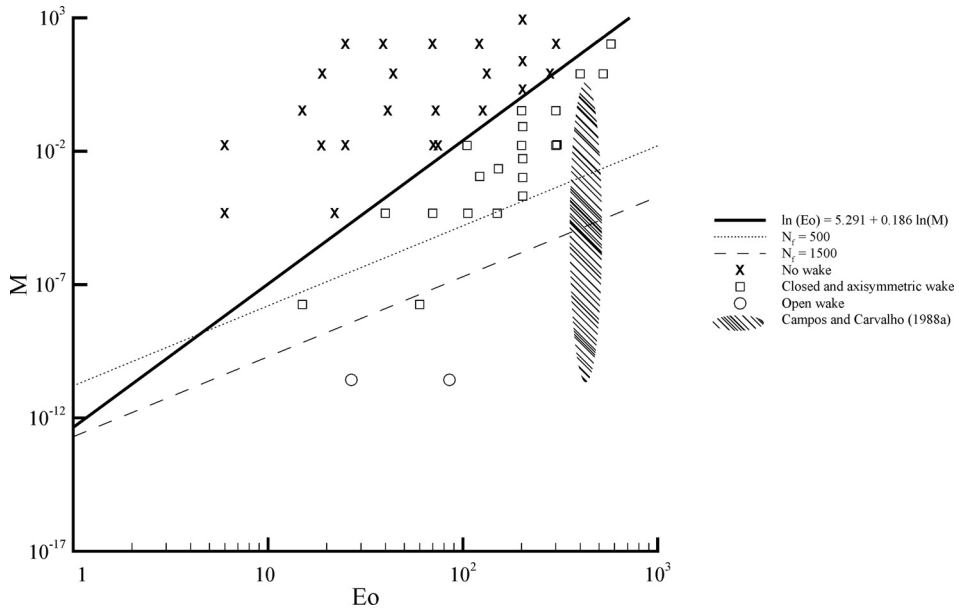

Fig. 9. Phase diagram of the existence and type of wake of Taylor bubbles rising through vertical columns of stagnant liquid. The data was extracted from the works of van Hout et al. (2002b), Shemer et al. (2007b), Taha and Cui (2006), Lu and Prosperetti (2008), Kang et al. (2010) and Araújo et al. (2012).

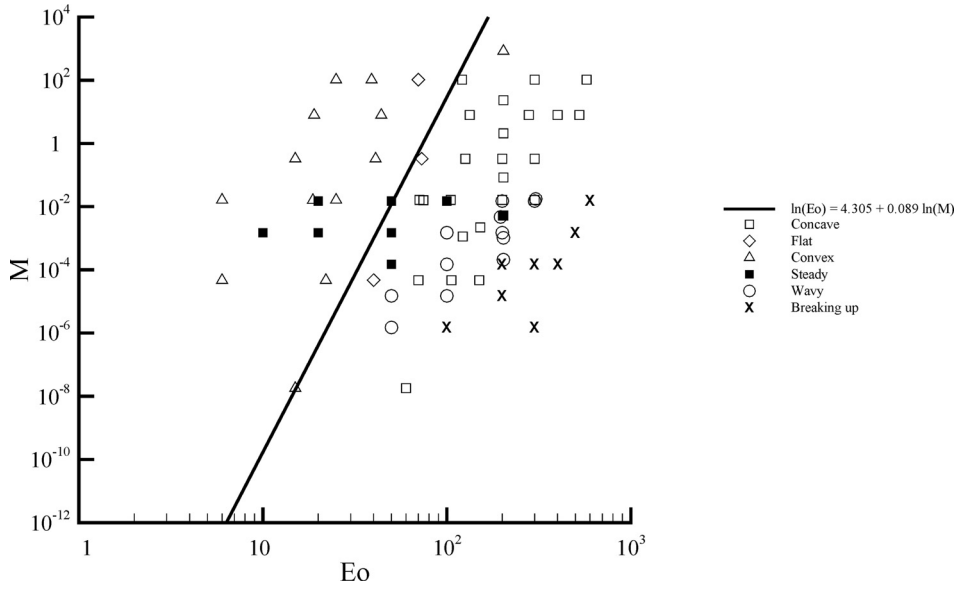

Fig. 10. Phase diagram of the shape of the rear of a Taylor bubble rising through vertical columns of stagnant liquid. The data was extracted from the works of Taha and Cui (2006), Lu and Prosperetti (2008), Kang et al. (2010) and Araújo et al. (2012).

different types of wakes was compared with the limits proposed by Campos and Carvalho (1988a) based on N_f values, in order to validate those limits beyond the estimated (from 100% water to 40% water/60% glycerol solutions) range of Morton and Eötvös numbers studied by those authors, represented by the hatchings.

From Fig. 9, it is noticeable that, as the Morton number increases, the wake starts to develop as for increasing values of the Eötvös number. The curve estimated by Araújo et al. (2012) for the wake formation, given by:

$$\ln(\mathrm{Eo}) = 5.291 + 0.186 \ln(\mathrm{M}), \tag{26}$$

is in agreement with the results presented in Fig. 9. As expected, for gradually higher Eo values, the wake flow pattern changes, and closed and axisymmetric wakes lose their symmetry, eventually opening. Moreover, the majority of the results from literature are in agreement with the classification proposed by Campos and Carvalho (1988a) for the wake flow pattern as a function of N_f: closed and axisymmetric wakes are mostly observed at the left of the laminar wake upper limit ($N_f = 500$), and all opened wakes fall at the right or in line with the turbulent wake one ($N_f = 1500$). Nevertheless, no data was found for closed and unaxisymmetric, *i.e.*, transitional wake, highlighting the shortage of studies that allow for a clear of the transition region.

In the data depicted on Fig. 10, the concept of steady bubble rears includes concave, convex and flat trailing edges. The steady concept is here used since some authors do not mention the specific shape of the bubble tail. Additionally, it should be added that the *breaking up* concept describes very unstable bubble rears where the formation of small gas bubbles is often observed. The shape of the bubble trailing edge varies from convex, to flat and then to concave as the Eötvös number increases. Further increase of this dimensionless group causes the bubble tail to

lose its steadiness, becoming wavy and eventually breaking up. As it was found for the transition between wake types, increasing the Morton number, results in transitions on the shape of the bubble rear occurring for higher values of Eo. Despite the good agreement between data, there seems to be some overlapping of the wavy behavior of the tail with the concave ones, which is probably related to the fact that the *wavy* concept has not been used by some authors. The curve estimated by Araújo et al. (2012) for transition between convex and concave tail, given by:

$$\ln(\mathrm{Eo}) = 4.305 + 0.089\ln(\mathrm{M}), \tag{27}$$

is in agreement with the data from literature.

Interesting phenomena, occurring at the rear of Taylor bubbles and regarding its shape, have been described by several authors. Goldsmith and Mason (1962) reported that, for viscous flow, *i.e.*, for low Reynolds regimes, although both ends of the bubble are spheroidal, the nose prolate and the rear typically oblate, small disturbance waves appeared at the beginning of the curvature of the bubble rear. Even for inertia-controlled regimes, if the bubble Reynolds number was low ($\mathrm{Re_{TB}} \in [25, 75]$), the bubble rear exhibited disturbances described by the authors as successive thick rings. Such behavior was also observed in the experiments of Polonsky et al. (1999a) and in the numerical study of Tomiyama et al. (1996). Furthermore, Liberzon et al. (2006), using digital image processing, observed that, for short Taylor air bubbles rising through vertical columns of water both stagnant and following co-currently, upward-propagating capillary waves appeared at the air-water interface. Those capillary waves are attributed to the oscillation of the bubble rear. The length of the capillary waves has an opposite behavior to that of the downward liquid velocity in the annular film, thus, as the downward liquid film flow increases towards the bubble rear, the length of the capillary waves is higher near the nose and lower at the bottom. Moreover, as the tube diameter or the liquid phase flow rate increases, the downward liquid film velocity also increases, resulting even shorter waves. Therefore, such waves appear only for short Taylor bubbles, since for longer ones the waves will be too short and, according to Liberzon et al. (2006), decay fast.

5. Individual Taylor bubbles in co-current flows

In gas–liquid slug flow, if the continuous phase is no longer stagnant but flowing liquid, besides buoyancy, the motion of the Taylor bubbles will depend on the liquid velocity.

Nicklin et al. (1962) studied experimentally the motion of single Taylor bubbles in stagnant and co-current flowing water, measuring the nose position and the bubble length from pictures taken by a camera moving upwards at the bubble speed – moving frame of reference, MFR. From the slope of the position *vs.* time curve, the authors obtained the bubble velocity. They reported that, for the case of a Taylor bubble rising in a flowing liquid, its absolute velocity should be expressed as the sum of the bubble velocity in stagnant liquid, U_∞, and a term proportional to the average liquid velocity, U_L:

$$U_{TB} = U_\infty + CU_L\ . \tag{28}$$

In their experiments, Nicklin et al. (1962) found the coefficient C to be 1.2 when the Reynolds number of the flowing liquid, Re_{U_L}, was higher than 8000, *i.e.*, for turbulent liquid flow, whereas, in the laminar regime, they reported C to be approximately 2. These results suggest that C corresponds to the ratio between the maximum or centerline liquid velocity, U_C, and U_L, both measured ahead of the bubble nose where the liquid is undisturbed.

Although the approach of Nicklin et al. (1962) neglected the effects of surface tension on bubble motion, the experimental study of Bendiksen (1984), extended for the case where these effects have a significant impact, confirmed the value of $C = 1.2$ for $\mathrm{Re}_{U_L} = [5000; 11000]$. The values of C proposed by Nicklin et al. (1962) for both laminar and turbulent regimes have been further validated by a myriad of other experimental (Nogueira et al., 2006a; Pinto et al., 2001; Polonsky et al., 1999b; Shemer, 2003; van Hout et al., 2002b) and numerical (Lu and Prosperetti, 2008; Mao and Dukler, 1991) works.

The problem of the rising velocity of Taylor bubbles in vertical columns of flowing liquids has also been addressed theoretically. On their study, Collins et al. (1978) reported a generic solution for laminar and turbulent regimes in the liquid phase:

$$U_{TB} = U_C + \sqrt{g.D}\ \phi\left(\frac{U_C}{\sqrt{g.D}}\right), \tag{29}$$

with ϕ indicating a functional dependency on the shape of the liquid velocity profile. For co-current slug flow in the inertia-controlled regime and $\mathrm{Re}_{U_L} > 4000$, *i.e.*, turbulent regime in the liquid, the authors showed that U_{TB} is given by:

$$U_{TB} = U_L\left(\frac{\ln \mathrm{Re}_{U_L} + 0.089}{\ln \mathrm{Re}_{U_L} - 0.74}\right) + 0.347\sqrt{gD} \times \emptyset\left\{\frac{U_L}{\sqrt{gD}}\frac{1.81}{\ln \mathrm{Re}_{U_L} - 0.74}\right\}, \tag{30}$$

whereas in the viscous-controlled laminar regime, *i.e.*, for $0 < \mathrm{Re}_{U_L} < 2100$, it is given by:

$$U_{TB} = 2U_L + 0.347\sqrt{gD} \times \emptyset\left\{\frac{2.39\ U_L}{\sqrt{gD}}\right\}. \tag{31}$$

Assuming potential axisymmetric flow and solving Stokes equation for the stream function, Collins et al. (1978) found the theoretical results obtained for turbulent regime, Eq. (30), to be in good agreement with the experimental value of $U_C/U_L = 1.22$, and close to that of Nicklin's, $C = 1.2$. The theoretical predictions for laminar regime were also in agreement with Collins et al. (1978) experimental data, but only when entrance effects were negligible, *i.e.*, for fully developed parabolic velocity profile. The results from Eq. (31) are also corroborated by Nicklin's equation using $C = 2.0$.

Thus, it is important to accurately determine the limits of the region in which transition from laminar to turbulent regime in the liquid phase occurs. Using a non-intrusive image analysis complemented with PIV measurements, Pinto et al. (2005) performed a study on the velocity of individual Taylor bubbles rising in vertical co-current liquid flow, and observed that transition in the bubble velocity occurred for $\mathrm{Re}_{U_L} \ll 2100$ (laminar regime). Such observation, besides being in agreement with the findings of Collins et al. (1978) and Polonsky et al. (1998), suggests that C does not depend solely on Re_{U_L}. Considering such observation, it was proposed the following empirical correlations to predict the velocity coefficient C:

$$\begin{aligned}
&C = 2.0 \pm 0.1, \ \text{for } \mathrm{Re}_{U_L}\mathrm{We}_{U_\infty}^{0.21}\left(\frac{U_L}{U_\infty}\right)^{0.28} < 1000;\\
&C = 2.08 - 1.38\times 10^{-4}\mathrm{Re}_{U_L}\mathrm{We}_{U_\infty}^{0.21}\left(\frac{U_L}{U_\infty}\right)^{0.28},\\
&\qquad \text{for } 1000 < \mathrm{Re}_{U_L}\mathrm{We}_{U_\infty}^{0.21}\left(\frac{U_L}{U_\infty}\right)^{0.28} < 6000;\\
&C = 1.2 \pm 0.1, \ \text{for } \mathrm{Re}_{U_L}\mathrm{We}_{U_\infty}^{0.21}\left(\frac{U_L}{U_\infty}\right)^{0.28} > 6000;
\end{aligned} \tag{32}$$

where We_{U_∞} is the Weber number for the bubble in stagnant fluid, given by $\mathrm{We}_{U_\infty} = \rho_L {U_\infty}^2 D/\sigma$.

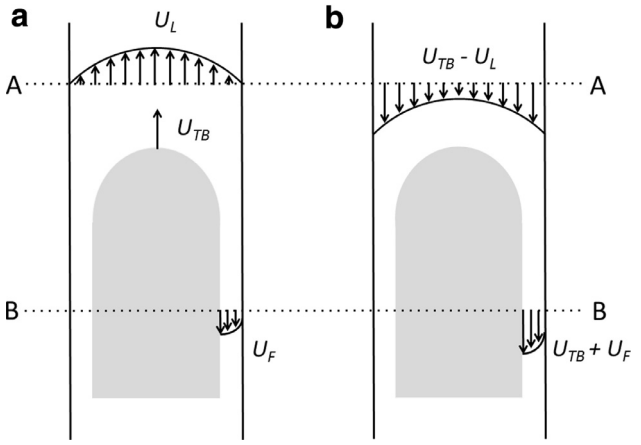

Fig. 11. Velocity patterns at planes A-A and B-B, in (a) a fixed frame of reference and in (b) a frame of reference moving with the Taylor bubble, for co-current slug flow conditions.

From the general flow description made previously for single Taylor bubbles rising in a vertical column of stagnant liquid, the majority of the hydrodynamic characteristics are maintained when the liquid phase is no longer quiescent. Hence, only the distinctive features between these two cases will be further assessed.

5.1. Ahead of the bubble nose

In co-current slug flow, and from a frame of reference moving with the bubble, the liquid ahead of it is moving downwards at a constant axial velocity of $(U_{TB} - U_L)$ until a certain distance from the bubble nose. Nogueira et al. (2006a) reported that the length above the bubble where the impact of its motion is felt, Z_A, increases for increasing liquid velocities.

The motion of the liquid phase also affects the shape of the bubble nose: its curvature radius was reported to be smaller for higher bubble velocities so as to compensate for the higher liquid flow rate, which, in a MFR, has an opposite direction to that of the bubble rise (Lu and Prosperetti, 2008; Nogueira et al., 2006a; Quan, 2011).

5.2. Film region

Fig. 11 illustrates the liquid velocity profiles ahead of the bubble nose and at the annular film region between the bubble and the tube wall, in (a) fixed frame of reference, FFR, and in (b) a MFR. Performing a material balance similar to the one described for stagnant liquid, the mean liquid film velocity is given by:

$$U_F = \frac{(U_{TB} - U_L)}{\left(1 - \frac{(R-\delta)^2}{R^2}\right)} - U_{TB}. \tag{33}$$

Thus, for systems with co-current liquid, the thickness of the annular fully developed film for laminar regime as derived by Brown (1965) becomes:

$$\delta = \left[\frac{3\upsilon_L}{2g(R-\delta)}\left((R-\delta)^2 U_{TB} - R^2 U_L\right)\right]^{1/3}. \tag{34}$$

In co-current flow, higher upward liquid velocities will cause the Taylor bubble to rise faster. As a result, larger thickness and downward velocities in the liquid film have been reported: for aqueous glycerol solutions of 0.016 Pa.s and 1170 kg/m^3, Nogueira et al. (2006a) found the bubble velocity to increase from 0.197 to 0.378 m/s and the film thickness from 1.84 to 2.58 mm, for an increase of U_L/U_∞ from 0 to 0.378, while increasing this ratio from 0.14 to 0.31 for a solution with 0.043 Pa.s and 1200 kg/m^3 promoted increases from 0.197 to 0.364 m/s in U_{TB}, and from 2.40 to 2.67 mm in δ.

As a consequence of this different flow configuration, the expression derived previously for the Reynolds number in the liquid film no longer holds. Substituting Eq. (33) in $\mathrm{Re}_F = U_F.\rho_L.\delta/\mu_L$ gives:

$$\mathrm{Re}_F = \frac{1}{\upsilon_L}\left[\left(\frac{R^2}{2R-\delta} - \delta\right) U_{TB} - \frac{R^2}{2R-\delta} U_L\right]. \tag{35}$$

While studying the flow in the annular film around Taylor bubbles, Nogueira et al. (2006a) found that, when the liquid phase is moving, longer bubbles are required in order for the laminar film to become fully developed, when compared with similar stagnant liquid systems ($Z*_{\text{stagnant}} < Z*_{\text{co-current}}$). From the axial velocity component obtained experimentally using simultaneously PIV and PST techniques, these authors estimated the value of $Z*$ for the same column and identical liquid solutions (viscosity of 0.043 Pa s): about $2.2D$ in stagnant conditions, while in the co-current case ($U_L = 0.074$ m/s) a value of $3.6D$ was obtained.

Under the assumption of no friction at the gas-liquid interface, the annular liquid film flows downwards supported by the shear stress on the tube wall. Nogueira et al. (2006a) observed experimentally that, in both stagnant and co-current conditions, the wall shear stress, τ_w, decreases with decreasing μ_L. Such results were expected since the wall shear stress is proportional to the shear rate, experienced by the fluid, being the coefficient its viscosity. By comparing the results from experiments performed in stagnant and co-current conditions for two different liquid viscosities, Nogueira et al. (2006a) found that, for the higher value of μ_L considered, the liquid velocity had little influence on τ_w, with the wall shear stress profiles being almost coincident. However, the results for the less viscous solution showed a clear departure of these profiles, suggesting that the influence of the liquid velocity on τ_w is significant when the viscosity of the liquid phase is low. Furthermore, when the liquid viscosity was low, the experimental results indicated an increase of τ_w with increasing liquid flow rates.

5.3. Wake region

In spite of the higher degree of flow complexity in co-current conditions and the influence of the liquid velocity in the overall features of slug flow, the flow patterns in the wake of a bubble rising in flowing liquid may also be divided into the same two boarder types as in the stagnant conditions: closed and open. Further away from the bubble trailing edge, the liquid velocity profile emerging from the wake develops to restore the main liquid profile.

Pinto et al. (1998) suggested that the flow pattern in the wake of Taylor bubbles rising in flowing liquids should be well characterized by Re_{V_L}, the Reynolds number of the flowing liquid based on the mean relative velocity of the liquid, V_L, *i.e.*, in a MFR. Such hypothesis is similar to that of Campos and Carvalho (1988a), who proposed that the wake flow pattern of Taylor bubble moving in stagnant liquids was a unique function of the inverse viscosity number. V_L is given by:

$$V_L = U_{TB} - U_L = (U_\infty + CU_L) - U_L = (\mathrm{C}-1)U_L + U_\infty, \tag{36}$$

yielding the following expression for Re_{V_L} in the inertia-controlled regime is:

$$\mathrm{Re}_{V_L} = \frac{V_L.\rho_L.D}{\mu_L} = \frac{[(\mathrm{C}-1)U_L + U_\infty]D}{\upsilon_L} = \frac{D(\mathrm{C}-1)U_L}{\upsilon_L} + 0.35\mathrm{N}_f. \tag{37}$$

Based on the work of Campos and Carvalho (1988a), Pinto et al. (1998) suggested the following limits for the flow patterns in the wake of a Taylor bubble rising co-currently with the liquid phase:

Type I – Laminar wake, $Re_{V_L} < 0.35 \times 500 < 175$

The wake is closed and axisymmetric with internal recirculatory flow.

Type II – Transitional wake, $175 < Re_{V_L} < 0.35 \times 1500 < 525$

The wake is still closed, but lacking in symmetry. Internal recirculatory flow is also observed.

Type III – Turbulent wake, $Re_{V_L} > 525$

The wake is open and perfectly mixed.

These empirical limits were first experimentally confirmed by Nogueira et al. (2006b).

Studying the characteristics of the wake of Taylor bubbles in Newtonian liquids -, for the same column and identical liquid solutions, Nogueira et al. (2006b) reported the wake length to be slightly higher in co-current conditions when compared with stagnant systems. Furthermore, for laminar and transitional wakes, this region length and volume were reported to increase with the decreasing impact of the viscous forces acting onto the liquid, *i.e.*, for increasing Re_{V_L}:

$$\frac{l_w}{D} = 3.60 \times 10^{-3} \, Re_{V_L} + 0.083, \tag{38}$$

$$\frac{V_w}{D} = 1.40 \times 10^{-3} \, Re_{V_L} - 0.022, \tag{39}$$

a similar dependence to that of these two features with N_f for bubbles flowing in stagnant liquids. The work of Nogueira et al. (2006b) corresponds to the first systematic characterization of the wake of Taylor bubbles in co-current slug flow.

Shemer et al. published several works on the structure of turbulent wakes of Taylor bubbles rising in stagnant and co-current liquid flows (Shemer, 2003; Shemer et al., 2005; Shemer et al., 2007b). Performing PIV measurements, these authors found that, if the background liquid flow is laminar and there is no effective mixing beyond the near wake region, the main liquid velocity profile is only fully restored at about 70*D* from the bubble trailing edge. However, if the background liquid flow is turbulent, the liquid behind the bubble undergoes transition between turbulent regimes, and while the mean velocity profile its restored at around 20–30*D* from the bubble bottom, the relaxation of the turbulent structure seems to require a longer distance, since the liquid in the wake passes through a partially laminarized domain during this transition (Shemer et al., 2007b). Nevertheless, further operating conditions should be evaluated in order to obtain more systematic data on co-current gas-liquid slug flow, particularly for the case of turbulent wakes, about which there is a considerable scarcity of available data.

Since the complete reestablishment of the velocity profile in the main liquid requires a certain length to be achieved, the distance from the Taylor bubble trailing edge needed to restore the undisturbed velocity profile, l_{min}, is an important parameter to be assessed. Nogueira et al. (2006b) reported that, for identical liquid solutions and low Re_{V_L} ranges, the l_{min} values obtained in co-current conditions are lower than in stagnant ones. Despite being in agreement with the findings of Pinto et al. (1998), these results are, once more, limited and should be extended to higher ranges of Re_{V_L} in order to ensure a complete understanding of this feature, due to its important role in continuous slug flow.

6. Interaction between Taylor bubbles

The rise of individual Taylor bubbles through a stagnant or co-current flowing liquid phase was addressed in the previous sections. However, in the majority of slug flow practical applications, long bubbles rise almost sequentially, with the gas phase being continuously fed. Provided that the distance between the bubbles is short enough, interaction between them occurs, eventually leading to coalescence.

As aforementioned, the motion of a Taylor bubble is influenced by the liquid velocity profile ahead of its nose. Moissis and Griffith (1962) were the first to investigate the development of continuous vertical slug flow, noticing that, when a short distance separates two bubbles, the trailing bubble rises faster eventually catching the leading one. Such behavior suggests that the flow pattern in the wake of the leading bubble is crucial for the velocity of the trailing one. Conducting experiments for air-water systems and turbulent flow, Moissis and Griffith (1962) found wake effects to be significant for large diameter tubes ($D \geq$ 1 in), with a minimum distance between bubbles of about 8–16*D*.

After conducting experiments with plastic bubbles and measuring the velocity profile behind them, Moissis and Griffith (1962) proposed a theoretical correlation for the dependence of the trailing bubble rise velocity, U_t, on the separation distance between bubbles, l, rising through quiescent liquid:

$$\frac{U_t}{U_l} = 1 + exp\left(-1.06\frac{l}{D}\right), \tag{40}$$

where U_l represents the velocity of the leading bubble. It should be emphasized that the first bubble of a train of bubbles is not affected by the motion of the following ones, and, thus, rises as an isolated Taylor bubble (Pinto and Campos, 1996).

The minimum separation distance between bubbles that ensures fully developed continuous slug flow (l_{min}), *i.e.*, the minimum length for which there is no interaction between bubbles, is an important parameter to be assessed, and two approaches have been proposed in order to predict it:

- In the first, the liquid film flowing downwards between the bubble and the tube wall is assumed to enter the rear of the leading bubble as a two-dimensional wall jet entering a large reservoir, and, thus, l_{min} is given by the distance at which the jet is absorbed by the liquid behind the bubble (Barnea and Brauner, 1985; Taitel et al., 1980);
- A different theoretical approach suggests that the liquid film promotes a well-mixed region at the leading bubble rear (wake), resulting in the relaxation of the wall boundary layer; in this case, l_{min} corresponds to the length needed to restore the main liquid velocity profile (Dukler et al., 1985).

Nevertheless, some of the assumptions underlying those approaches are not entirely correct. In the second, for instance, the wake is considered a highly turbulent mixing zone, which is only true for $N_f >$ 1500 (Campos and Carvalho, 1988a,b).

Furthermore, both approaches assumed that the maximum liquid velocity at any cross-section is located at the center of the tube. However, for some distance behind the leading bubble, the velocity profile fluctuates and the radial position of the maximum liquid velocity may change as the distance from the leading bubble trailing edge increases (Pinto and Campos, 1996; Shemer and Barnea, 1987). This can occur due to turbulence ahead of the trailing bubble nose, or if the wake of the leading one is unaxisymmetric. The nose of the trailing bubble has also been reported to distort as it approaches the rear of the bubble ahead of it (Pinto and Campos, 1996; Shemer and Barnea, 1987; Tudose and Kawaji, 1999). Such phenomena is the result of the maximum liquid velocity fluctuations: the bubble “searches” the lower pressure paths to rise throughout the pipe with its nose being “attracted” to the higher upward velocity liquid (Pinto et al., 1998; Shemer et al., 2007a), resulting in an undulating nose shape.

As with single Taylor bubbles, different hydrodynamic behaviors arise depending on whether the bubbles flow through stagnant or moving liquids, and so both scenarios will be addressed separately.

6.1. Stagnant liquid

Campos and Carvalho (1988a) suggested the flow pattern in the wake of a Taylor bubble rising in stagnant liquid to be a unique function of N_f. Pinto and Campos (1996) found this dimensionless number to be also relevant in bubble-to-bubble interaction, validating the hypothesis of Moissis and Griffith (1962) that the flow at the leading bubble wake influences the motion of the bubble behind it.

Pinto and Campos (1996) studied the coalescence of pairs of Taylor bubbles rising in vertical columns of stagnant liquids, for a wide range of liquid viscosities and three tube diameters. The authors determined the distances between bubbles for which their relative velocity was zero, *i.e.*, for which there was no interaction, and identified three ranges of N_f values corresponding to the different regimes in the wake of the leading bubble, as defined by Campos and Carvalho (1988a):

Laminar wake, 100 < N_f < 500 - l_{min}/D varies linearly with N_f:

$$\frac{l_{min}}{D} = 1.46 + 4.75 \times 10^{-3}\ N_f; \tag{41}$$

Transitional wake, 500 < N_f < 1500 - l_{min}/D varies linearly with N_f:

$$\frac{l_{min}}{D} = 6.92 \times 10^{-1} + 7.90 \times 10^{-3}\ N_f; \tag{42}$$

Turbulent wake, N_f > 1500 - l_{min}/D is constant and given by:

$$\frac{l_{min}}{D} = 12.5, \tag{43}$$

which corresponds to the midpoint of the range reported by Moissis and Griffith (1962) for air–water systems: $l_{min}/D \in [8; 16]$.

After determining the minimum distance for which the bubbles do not interact, Pinto and Campos (1996) compared l_{min} with the length of the wake of the leading bubble. From this analysis resulted an interesting finding: despite the flow pattern on the leading bubble wake, the distance between consecutive Taylor bubbles can be divided in two parts:

- **$0 < l/l_{min} < 0.24$: Portion of l_{min} occupied by the wake of the leading bubble.** If the nose of the trailing bubble rises inside this section, the interaction between bubbles is strong. Pinto and Campos (1996) reported the variation of the ratio between the velocities of the trailing and leading bubbles with l/l_{min} to be well-described by:

$$\frac{U_t}{U_l} = -11.4\frac{l}{l_{min}} + 4.24; \tag{44}$$

- **$l/l_{min} > 0.24$: Portion of l_{min} where the main liquid velocity profile is being restored**. The interaction between bubbles is weaker if the nose of the trailing bubble rises inside this region. In this section, the following expression describes the dependence of U_t/U_l with l/l_{min} (Pinto and Campos, 1996):

$$\frac{U_t}{U_l} = 2.01 - 1.96\frac{l}{l_{min}} + 0.95\left(\frac{l}{l_{min}}\right)^2. \tag{45}$$

The experimental results of Shemer et al. (2007a), who used image processing techniques combined with PIV measurements to study the motion of consecutive Taylor bubbles rising through vertical columns of stagnant and co-current flowing water, are in agreement with the findings of Pinto and Campos (1996). Shemer and colleagues observed that the merger of two consecutive bubbles was dependent on the initial separation distance between them. They suggested that, for flowing liquid, coalescence would not be found for bubbles initially at more than 7–10D.

Applying CFD tools to study the interaction between two Taylor bubbles rising in vertical columns of stagnant liquids, and simulating systems with flow conditions that ensured laminar wakes, Araújo et al. (2013b) identified a sharpening-flattening behavior of the trailing bubble nose, as well as a significant deformation of the leading bubble bottom with the decrease of the distance between them. These features were particularly evident for the lower M values or increasing values of Eo. The alteration of the bubbles shape during their approach has an impact on the characteristics of the developing liquid film surrounding the trailing bubble, as well as in the dimensions of its wake. Araújo et al. (2013b) reported a general tendency of the length required to have a fully developed film, $Z*$, of the film thickness and of the velocity in this region to increase as the separation between bubbles decreases. A similar tendency was obtained for the length and volume of the trailing bubble wake. Moreover, representing the numerical U_t/U_l data as a function of the dimensionless separation distance between bubbles, l/D, Araújo et al. (2013b) detected the existence of two regions – an accelerating and a decelerating zone – for which they presented fitting equations (Eqs. (46) and (47), respectively) and the respective parameters for the pairs of M and Eo under study (a and b for the accelerating region; a', b' and c' for the decelerating one). The authors also shown that, if Eo < 90 and M $\geq 1.64 \times 10^{-2}$, it is possible to determine the acceleration zone from single bubble data. These findings are worth mentioned due to their potential used in Slug Flow Simulators.

$$\frac{U_t}{U_l} = 1 + a.\ exp\left(-b\frac{l}{D}\right). \tag{46}$$

$$\frac{U_t}{U_l} = \sqrt{a' + b'\left(\frac{l}{D}\right) + c'\left(\frac{l}{D}\right)\left[\ln\left(\frac{l}{D}\right) - 1\right]}. \tag{47}$$

6.2. Co-current flow

In continuous co-current slug flow, the complexity of the wake flow increases, affecting the interaction between consecutive Taylor bubbles, due to the dependence of the trailing bubble motion on the velocity profile of the liquid emerging from the wake of the leading one.

Let us consider the case where the liquid flows in laminar regime. If the velocity profile emerging from the wake is (almost) uniform, then, its magnitude along the entire region where the liquid velocity profile is restored is smaller than the maximum liquid velocity in the laminar parabolic profile, $2U_L$. In such conditions, the velocity of the leading bubble, whose nose travels through the undisturbed laminar liquid flow, is higher than that of the trailing one, and the distance between bubbles increases until the nose of the trailing one is no longer inside the reattachment profile region, with no coalescence occurring.

Nevertheless, if the velocity in the emerging liquid velocity profile somewhere in the cross-section is higher than $2U_L$, the trailing bubble nose traveling inside the reattachment profile region will have a velocity greater than that found ahead of the nose of the leading one. The distance between bubbles will, then, decrease throughout their rise, and the bubbles will eventually merge.

As for single Taylor bubbles rising through vertical columns of moving liquids, there is a considerable scarcity of data on the coalescence of two Taylor bubbles rising in such conditions. The work of Pinto et al. (1998) on the coalescence of pairs of bubbles rising through a co-current flowing liquid, either for laminar or turbulent liquid flow, in inertia-controlled regime (N_f > 300) and for

turbulent wake flow ($Re_{V_L} > 525$), stands out as the most systematic study published on this subject.

Pinto et al. (1998) reported that, if the flow regime in the main liquid is turbulent, no interaction occurs for distances between the trailing bubble nose and the leading bubble bottom equal or higher to 5*D*, regardless of Re_{U_L}. For smaller distances, a steep increase of U_t/U_l is observed, indicating that $l_w \sim l_{min}$ regardless of the gas-liquid flow conditions, leading to the coalescence of the bubbles.

If the liquid flow pattern is laminar, however, two situations may occur depending on the ratio between the average velocity in the fully developed film around the leading bubble, U_F, and the average velocity of the main liquid flow, U_L:

- if $U_F/U_L > 25$, Pinto et al. (1998) reported l_{min} to be constant and approximately 10*D*, regardless of the liquid flow regime;
- for $U_F/U_L < 25$ and an initial distance between bubbles longer than the length of the wake of the leading one, such distance will increase during the rise, preventing coalescence from happening (Pinto et al., 1998).

The same authors extended their work for a train of Taylor bubbles rising in the same conditions as the two bubbles in their 1998 study (Pinto et al., 2001). The conclusions from Pinto et al. (2001) confirmed the results obtained for two bubbles.

Interaction curves depicting the evolution of the ratio between the velocities of the trailing and the leading bubbles, $U_t/U_l \sim U_t/U_{TB}$, with the separation distance between them are useful to understand the interaction process in continuous slug flow. The influence of the liquid phase velocity on the coalescence process, for instance, was assessed in Araújo et al. (2015) CFD study using bubble-to-bubble interaction curves obtained in stagnant and co-current liquid flow configurations. These authors found that, although these curves followed the typical accelerating-decelerating trend reported by Araújo et al. (2013b), its magnitude decreases when the liquid is no longer quiescent. However, the distance over which the trailing bubble velocity gradually increases - acceleration region -, is longer for higher liquid flow rates.

6.3. Continuous slug flow

In fully developed continuous slug flow, no interaction between consecutive Taylor bubbles occurs. The bubbles rise at the same translational velocity (well described by Nicklin et al. (1962) equation) with the length of the liquid slugs between them remaining constant and higher than l_{min}.

The existence of a fully developed continuous slug flow remains debatable (Araújo et al., 2013b; Shemer et al., 2007a), since, at the tube inlet, the distance between bubbles is usually inferior to l_{min}, with the nose of the trailing one travelling inside the wake of the bubble ahead, or in its length of influence. As a result, coalescence between bubbles in the entrance region will be observed, with an alteration of the flow pattern along the tube. From the bubbles merger, longer ones arise, as well as longer liquid slugs, and, hence, a decline of the coalescence frequency occurs until steady state is achieved somewhere along the tube. The portion of tube required for the entrance effects to be no longer detected is usually designated as entrance length, l_e, which strongly depends on the range of superficial velocities of the gas and liquid phases (Mayor et al., 2008a, 2007a, 2008c, 2007b). As it can be inferred from the previous description, very long tubes are required to achieve fully developed continuous slug flow.

Further contributing to the difficulty in obtaining such steady flow pattern in real systems is the expansion of the gas phase caused by the pressure changes along the pipe, particularly in vertical tubes, that induces the bubble volume to increase, affecting its motion. Several of the experimental and numerical works found in the literature, that provide important understanding on the characteristics of continuous co-current vertical slug flow, have neglected gas expansion along the vertical pipe (Barnea and Taitel, 1993; Hasanein et al., 1996; Pinto et al., 2001; Van Hout et al., 2001, 2002a, 2003). Implementing a simulation approach, Mayor et al. (2008b) reported this to be an acceptable assumptions since gas expansion only accounts for a slight decrease in the coalescence phenomenon.

Mayor et al. published a collection of systematic studies on the hydrodynamics of gas-liquid slug flow along vertical pipes. Their experimental and numerical work bridges three different scenarios - fully turbulent regime in the main liquid and in the near-wake bubble region (Mayor et al., 2008a, 2007b), fully laminar regime (Mayor et al., 2007a) and a mixed case of laminar flow in the main liquid and turbulent regime in the near-wake region (Mayor et al., 2008c) -, containing detailed data on continuous slug flow. Based on their experimental data, obtained from non-intrusive image analysis, the authors proposed empirical correlations for bubble-to-bubble interaction, relating the *i*th trailing bubble velocity with the liquid slug length ahead of it, $l_{s,\ i-1}$. Graphical comparison between the authors' correlations for the three scenarios can be observed in Fig. 12, where $U_{t,\ i}$ is normalized by the experimental average upward isolated bubble velocity ($U_{TB}^{exp.}$) and the slug length normalized by the column internal diameter (*D*).

The data from Fig. 12 suggests the mixed scenario to be an intermediate between the fully turbulent and the fully laminar regimes, in line with the experimental findings of Mayor et al. (2008a, 2007a, 2008c), who observed strong interaction between consecutive bubbles for distances inferior to 3–4*D* in the mixed scenario, whereas for the turbulent flow pattern in the liquid and in the wake l_{min}=8–10*D*, and for the fully laminar scenario l_{min}=2*D*.

Mayor et al. (2008c) also reported, for the range of U_G and U_L indicated in Fig. 12, the length of column needed to achieve fully developed continuous slug flow, l_e: between 50*D* and 70*D* in fully turbulent regime, 70–100*D* for the fully laminar scenario, and 50–80*D* for the mixed one. Having reached steady state flow, further assessment of the impact of the flow pattern in the main liquid and in the near-wake bubble region showed the mixed scenario to be almost always a midpoint between the extreme cases. For fully developed flow and taking the mixed case as reference, bubble velocity is higher when the regime in the main liquid and wake is laminar and lower when the flow pattern in both regions is turbulent. Regarding the lengths of the bubble and of the liquid slug, higher values appear for fully turbulent regime and lower ones for fully laminar, although it should be noticed that, for the bubble length, the values obtained by Mayor et al. (2007a, 2008c) when the flow pattern is laminar in the liquid and in the wake are very close to those of the mixed scenario.

7. Conclusions

Slug flow is characterized by the rise of long, bullet-shaped gas bubbles – Taylor bubbles -, which occupy almost the tube entire cross-section, being separated by liquid slugs. Besides its numerous applications in industrial processes, slug flow is also observed in oil extraction, and on physiological and geological systems. However, slug flow complexity, due to its aperiodic behavior in space and time, often exposes the limitations of purely experimental studies, which should be complemented with numerical ones. The need to systematize the large amount of data published on the subject since the 1940s constitute the motivation for this review on vertical gas–liquid slug flow.

To accurately model slug flow it is first essential to understand the motion of single Taylor bubbles rising through stagnant liquids. Throughout its rise, the bubble is influenced by gravitational, inertial, viscous and interfacial forces. Neglecting gas expansion,

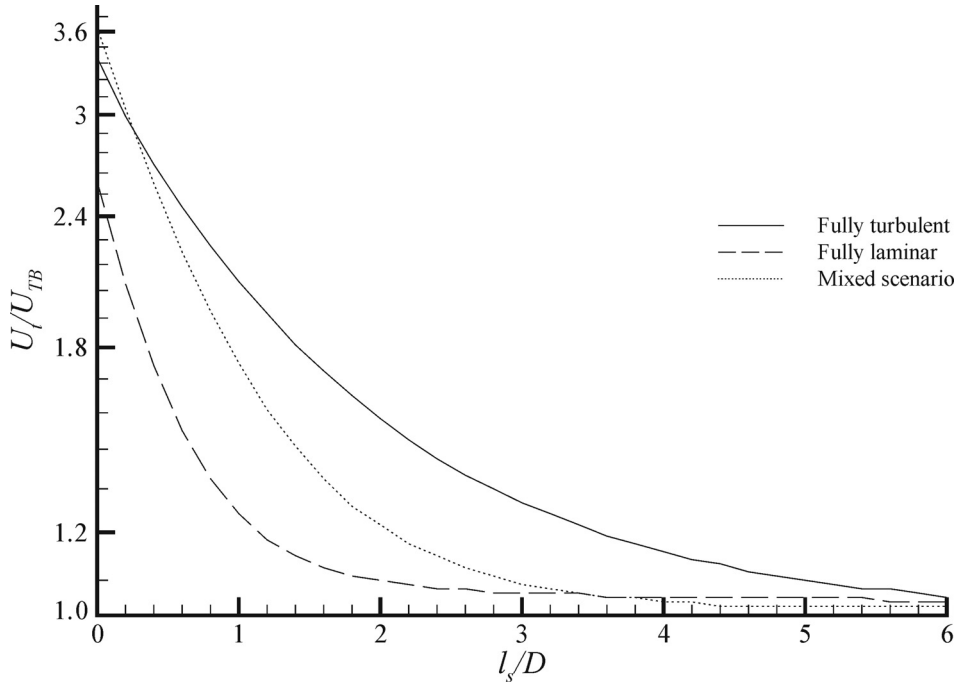

Fig. 12. Comparison between the bubble-to-bubble interaction curves for turbulent regime in the main liquid and in the near-wake region for $\boldsymbol{U_L}$ and $\boldsymbol{U_G} \in$ [0.10; 0.50] m/s (after Mayor et al. (2008a)), laminar regime in the main liquid and in the near-wake region for $\boldsymbol{U_L}$ and $\boldsymbol{U_G} \in$ [0.05: 0.20] m/s (after Mayor et al. (2007a)), and laminar regime in the main liquid and turbulent regime in the near-wake region for $\boldsymbol{U_L} \in$ [0.10; 0.30] m/s and $\boldsymbol{U_G} \in$ [0.10; 0.40] (after Mayor et al. (2008c)).

several authors reported $\mathrm{Fr} = f(\mathrm{Eo}, \mathrm{M})$ to be sufficient for the characterization of the rise of single Taylor bubble in stagnant liquid conditions (Collins et al., 1978; Taha and Cui, 2006; White and Beardmore, 1962). In the literature, the bubble velocity and shape, the velocity in the annular film established between the bubble and the tube wall, as well as its thickness, and the dimensions of the bubble wake are fully characterized for laminar regime and $N_f < 500$. For higher values of the inverse viscosity number, however, Taylor bubbles lose their symmetry, and so, if a numerical approach is adopted, 3D studies are mandatory to ensure a detailed understanding of the flow features. Thus, for $N_f > 500$, scarce data is found in literature, being the numerical data available unreliable without experimental confirmation.

If the liquid phase is flowing at a mean velocity U_L, U_{TB} will be given by the sum of the bubble drift velocity, U_∞, and a term proportional to the liquid velocity, C, representing the ratio between the centerline liquid velocity, U_C, and U_L: $U_{TB} = U_\infty + CU_L$. In co-current slug flow, the Taylor bubble motion depends additionally on the Reynolds number of the flowing liquid. Nevertheless, this significant increase of the parameter space does not constitute an extra difficulty for the determination of the bubble velocity, since Nicklin's equation allows for its determination from the bubble velocity in stagnant liquid conditions. It should be emphasized the considerable shortage of systematic data available in literature for other slug flow characteristics (*e.g.*, wake size, film thickness, …) for transitional and turbulent liquid flow.

In several slug flow processes, the gas phase is continuously fed and the bubbles rise consecutively. The distance between bubbles at the inlet is usually inferior to l_{min} and coalescence is observed. From the bubbles merger, longer ones arise, as well as longer liquid slugs. Coalescence frequency decreases until developed flow is achieved somewhere along the tube. For two Taylor bubbles rising consecutively in stagnant liquid, interaction velocity was systematically studied and determined for $N_f < 500$. Nevertheless, although some data is also available in literature for bubble-to-bubble interaction in quiescent conditions at $N_f > 500$, besides the results of Araújo et al. (2013b), there is a considerable scarcity of data for the co-current flow configuration.

Future work on vertical gas-liquid slug flow should also focus on the hydrodynamics of the liquid film surrounding the Taylor bubble, as well as further experimental studies that ensure a clear delimitation of the transition region in the film. Moreover, flow characteristics for individual and consecutive Taylor bubbles should also be assessed at $N_f > 500$, region for which there is a considerable lack in available data. This is particularly evident for co-current flow, whose features should be deeply investigated in order to validate the available data for low Reynolds regimes, and to expand the operating conditions ensuring complete understating of its characteristics in transitional and turbulent regimes.

References

Abdulkadir, M., Hernandez-Perez, V., Lo, S., Lowndes, I., Azzopardi, B., 2015. Comparison of experimental and computational fluid dynamics (CFD) studies of slug flow in a vertical riser. Exp. Therm. Fluid Sci. 68, 468–483.
Angeli, P., Gavriilidis, A., 2008. Hydrodynamics of Taylor flow in small channels: a review. Proc. Inst. Mech. Eng. Part C J. Mech. Eng. Sci. 222, 737–751.
Araújo, J., Miranda, J., Campos, J., 2013a. Simulation of slug flow systems under laminar regime: hydrodynamics with individual and a pair of consecutive Taylor bubbles. J. Pet. Sci. Eng. 111, 1–14.
Araújo, J., Miranda, J., Campos, J., 2015. CFD Study of the hydrodynamics of slug flow systems: interaction between consecutive Taylor bubbles. Int. J. Chem. Reactor Eng. 13, 541–549.
Araújo, J.D.P., Miranda, J.M., Campos, J.B.L.M., 2013b. Flow of two consecutive Taylor bubbles through a vertical column of stagnant liquid—A CFD study about the influence of the leading bubble on the hydrodynamics of the trailing one. Chem. Eng. Sci. 97, 16–33.
Araújo, J.D.P., Miranda, J.M., Pinto, A.M.F.R., Campos, J.B.L.M., 2012. Wide-ranging survey on the laminar flow of individual Taylor bubbles rising through stagnant Newtonian liquids. Int. J. Multiph. Flow 43, 131–148.
Barnea, D., 1987. A unified model for predicting flow-pattern transitions for the whole range of pipe inclinations. Int. J. Multiph. Flow 13, 1–12.
Barnea, D., Brauner, N., 1985. Holdup of the liquid slug in two phase intermittent flow. Int. J. Multiph. Flow 11, 43–49.
Barnea, D., Taitel, Y., 1993. A model for slug length distribution in gas-liquid slug flow. Int. J. Multiph. Flow 19, 829–838.
Barr, G., 1926. The air-bubble viscometer. Lond., Edinb., Dublin Philos. Mag. J. Sci. 1, 395–405 XXXI.

Batchelor, G., 1967. An Introduction to Fluid Dynamics. Cambridge University Press, Cambridge.

Bellara, S.R., Cui, Z., Pepper, D.S., 1997. Fractionation of BSA and Lysozyme using gas-sparged ultrafiltration in hollow fiber membrane modules. Biotechnol. Prog. 13, 869–872.

Bendiksen, K.H., 1984. An experimental investigation of the motion of long bubbles in inclined tubes. Int. J. Multiph. Flow 10, 467–483.

Bendiksen, K.H., 1985. On the motion of long bubbles in vertical tubes. Int. J. Multiph. Flow 11, 797–812.

Bi, H., 1999. Pressure and voidage fluctuations in slugging fluidized beds. Can. J. Chem. Eng. 77, 568–572.

Braak, E., Alliet, M., Schetrite, S., Albasi, C., 2011. Aeration and hydrodynamics in submerged membrane bioreactors. J. Membr. Sci. 379, 1–18.

Bretherton, F., 1961. The motion of long bubbles in tubes. J. Fluid Mech. 10, 166–188.

Brötz, W., 1954. Über die Vorausberechnung der Absorptionsgeschwindigkeit von Gasen in strömenden Flüssigkeitsschichten1. Chem. Ing. Tech. 26, 470–478.

Brown, R., 1965. The mechanics of large gas bubbles in tubes: I. Bubble velocities in stagnant liquids. Can. J. Chem. Eng. 43, 217–223.

Bugg, J., Mack, K., Rezkallah, K., 1998. A numerical model of Taylor bubbles rising through stagnant liquids in vertical tubes. Int. J. Multiph. Flow 24, 271–281.

Bugg, J.D., Saad, G.A., 2002. The velocity field around a Taylor bubble rising in a stagnant viscous fluid: numerical and experimental results. Int. J. Multiph. Flow 28, 791–803.

Campos, J.B.L.M., Carvalho, J.R.F.G.d., 1988a. An experimental study of the wake of gas slugs rising in liquids. J. Fluid Mech. 196, 27–37.

Campos, J.B.L.M., Carvalho, J.R.F.G.d., 1988b. Mixing induced by air slugs rising in narrow columns of water. Chem. Eng. Sci. 43, 1569–1582.

Cassidy, D.A., Edwards, J.R., Tian, M., 2009. An investigation of interface-sharpening schemes for multi-phase mixture flows. J. Comput. Phys. 228, 5628–5649.

Clarke, A., Issa, R., 1997. A numerical model of slug flow in vertical tubes. Comput. Fluids 26, 395–415.

Collins, R., Moraes, F.F.D., Davidson, J.F., Harrison, D., 1978. The motion of a large gas bubble rising through liquid flowing in a tube. J. Fluid Mech. 89, 497–514.

Cook, M., Behnia, M., 2000. Slug length prediction in near horizontal gas–liquid intermittent flow. Chem. Eng. Sci. 55, 2009–2018.

Cui, Z., Chang, S., Fane, A., 2003. The use of gas bubbling to enhance membrane processes. J. Membr. Sci. 221, 1–35.

Davies, R., Taylor, G., 1950. The mechanics of large bubbles rising through extended liquids and through liquids in tubes. Proc. R. Soc. Lond. A: Math., Phys. Eng. Sci. R. Soc. 375–390.

DeJesus, J., Ahmad, W., Kawaji, M., 2012. Experimental study of flow structure in vertical slug flow. Multiph. Flow.

Do Amaral, C., Alves, R., Da Silva, M., Arruda, L., Dorini, L., Morales, R., Pipa, D., 2013. Image processing techniques for high-speed videometry in horizontal two-phase slug flows. Flow Meas. Instrum. 33, 257–264.

Dukler, A., Bergelin, O.P., 1952. Characteristics of flow-in falling liquid films. Chem. Eng. Prog. 48, 557–563.

Dukler, A.E., Hubbard, M.G., 1975. A model for gas–liquid slug flow in horizontal and near horizontal tubes. Ind. Eng. Chem. Fundam. 14, 337–347.

Dukler, A.E., Maron, D.M., Brauner, N., 1985. A physical model for predicting the minimum stable slug length. Chem. Eng. Sci. 40, 1379–1385.

Dumitrescu, D.T., 1943. Strömung an einer Luftblase im senkrechten Rohr. ZAMM - J. Appl. Math. Mech. / Z. Angew. Math. Mech. 23, 139–149.

Elperin, T., Fominykh, A., 1997. Optimization of gas hydrate reactors with slug flow. Int. Commun. Heat Mass Transf. 24, 999–1008.

Fabre, J., Liné, A., 1992. Modeling of two-phase slug flow. Annu. Rev. Fluid Mech. 24, 21–46.

Fernandes, R., Semiat, R., Dukler, A., 1983. Hydrodynamic model for gas–liquid slug flow in vertical tubes. AIChE J. 29, 981–989.

Fulford, G.D., 1964. The flow of liquids in thin films. Adv. Chem. Eng. 151–236.

Funada, T., Joseph, D., Maehara, T., Yamashita, S., 2005. Ellipsoidal model of the rise of a Taylor bubble in a round tube. Int. J. Multiph. Flow 31, 473–491.

Ghosh, R., Cui, Z., 1999. Mass transfer in gas-sparged ultrafiltration: upward slug flow in tubular membranes. J. Membr. Sci. 162, 91–102.

Goldsmith, H., Mason, S., 1962. The movement of single large bubbles in closed vertical tubes. J. Fluid Mech. 14, 42–58.

Gupta, R., Fletcher, D., Haynes, B., 2010. Taylor flow in microchannels: a review of experimental and computational work. J. Comput. Multiph. Flows 2, 1–31.

Hall, A., 1997. Flow pattern in three-phase gas flows of oil, water and gas. In: Proceedings of the 8th International Conference Multiphase'97. Cannes, France.

Hao, Y., Prosperetti, A., 2004. A numerical method for three-dimensional gas–liquid flow computations. J. Comput. Phys. 196, 126–144.

Hasanein, H., Tudose, G., Wong, S., Malik, M., Esaki, S., Kawaji, M., 1996. Slug flow experiments and computer simulation of slug length distribution in vertical pipes. Am. Inst. Chem. Eng., New York, NY (United States).

Hattori, S.I., 1935. On the motion of a cylindrical bubble in a tube and its application to the measurement of the surface tension of a liquid. Report of the Aeronautical Research Institute of Tokyo Imperial University 9 (115), 159.

Hayashi, K., Kurimoto, R., Tomiyama, A., 2010. Dimensional analysis of terminal velocity of a Taylor bubble in a vertical pipe. Multiph. Sci. Technol. 22.

Hayashi, K., Kurimoto, R., Tomiyama, A., 2011. Terminal velocity of a Taylor drop in a vertical pipe. Int. J. Multiph. Flow 37, 241–251.

Hewitt, G.F., 1970. Annular Two-phase Flow. Pergamon Press, Oxford.

Ishii, M., 1975. Thermo-fluid dynamic theory of two-phase flow. NASA STI/Recon Technical Report A 75, 29657.

James, M., Lane, S., Chouet, B., Gilbert, J., 2004. Pressure changes associated with the ascent and bursting of gas slugs in liquid-filled vertical and inclined conduits. J. Volcanol. Geotherm. Res. 129, 61–82.

James, M.R., Llewellin, E.W., Lane, S.J., 2011. Comment on "It takes three to tango: 2. Bubble dynamics in basaltic volcanoes and ramifications for modeling normal Strombolian activity. J. Geophys. Res.: Solid Earth 116.

Joseph, D.D., 2003. Rise velocity of a spherical cap bubble. J. Fluid Mech. 488, 213–223.

Kang, C.-W., Quan, S., Lou, J., 2010. Numerical study of a Taylor bubble rising in stagnant liquids. Phys. Rev. E 81, 066308.

Kapitsa, P.L., Kapitsa, S.P., 1949. Wake flow of thin sheets of a viscous fluid. J. Exptl. Theor. Phys. URSS 19 (105).

Kawaji, M., DeJesus, J., Tudose, G., 1997. Investigation of flow structures in vertical slug flow. Nucl. Eng. Des. 175, 37–48.

Kay, J.M., Nedderman, R.M., 1985. Fluid Mechanics and Transfer Processes. CUP Archive.

Kurimoto, R., Hayashi, K., Tomiyama, A., 2013. Terminal velocities of clean and fully-contaminated drops in vertical pipes. Int. J. Multiph. Flow 49, 8–23.

Laird, A., Chisholm, D., 1956. Pressure and forces along cylindrical bubbles in a vertical tube. Ind. Eng. Chem. 48, 1361–1364.

Li, Q., Cui, Z., Pepper, D., 1997. Effect of bubble size and frequency on the permeate flux of gas sparged ultrafiltration with tubular membranes. Chem. Eng. J. 67, 71–75.

Liberzon, A., Guala, M., Kinzelbach, W., Tsinober, A., 2006. On turbulent kinetic energy production and dissipation in dilute polymer solutions. Phys. Fluids (1994-present) 18, 125101.

Llewellin, E.W., Del Bello, E., Taddeucci, J., Scarlato, P., Lane, S.J., 2012. The thickness of the falling film of liquid around a Taylor bubble. Proc. R. Soc. Lond. A: Math., Phys. Eng. Sci 468 (2140), 1041–1064.

Lu, X., Prosperetti, A., 2008. A numerical study of Taylor bubbles. Ind. Eng. Chem. Res. 48, 242–252.

Mandal, T., Das, G., Das, P., 2007. Prediction of rise velocity of a liquid Taylor bubble in a vertical tube. Phys. Fluids (1994-present) 19, 128109.

Mandal, T., Das, G., Das, P., 2009. Liquid Taylor bubbles rising in a vertical column of a heavier liquid: an approximate analysis. J. Fluids Eng. 131, 011303.

Mao, Z.-S., Dukler, A., 1989. An experimental study of gas-liquid slug flow. Exp Fluids 8, 169–182.

Mao, Z.-S., Dukler, A.E., 1991. The motion of Taylor bubbles in vertical tubes—II. Experimental data and simulations for laminar and turbulent flow. Chem. Eng. Sci. 46, 2055–2064.

Maxworthy, T., 1967. A note on the existence of wakes behind large, rising bubbles. J. Fluid Mech. 27, 367–368.

Mayer, M., Braun, R., Fuchs, W., 2006. Comparison of various aeration devices for air sparging in crossflow membrane filtration. J. Membr. Sci. 277, 258–269.

Mayor, T., Ferreira, V., Pinto, A., Campos, J., 2008a. Hydrodynamics of gas–liquid slug flow along vertical pipes in turbulent regime–An experimental study. Int. J. Heat Fluid Flow 29, 1039–1053.

Mayor, T., Pinto, A., Campos, J., 2007a. Hydrodynamics of gas–liquid slug flow along vertical pipes in the laminar regime experimental and simulation study. Ind. Eng. Chem. Res. 46, 3794–3809.

Mayor, T., Pinto, A., Campos, J., 2008b. On the gas expansion and gas hold-up in vertical slugging columns—A simulation study. Chem. Eng. Process. 47, 799–815.

Mayor, T., Pinto, A., Campos, J., 2008c. Vertical slug flow in laminar regime in the liquid and turbulent regime in the bubble wake—comparison with fully turbulent and fully laminar regimes. Chem. Eng. Sci. 63, 3614–3631.

Mayor, T.S., Pinto, A., Campos, J., 2007b. Hydrodynamics of gas–liquid slug flow along vertical pipes in turbulent regime: a simulation study. Chem. Eng. Res. Des. 85, 1497–1513.

Moissis, R., Griffith, P., 1962. Entrance effects in a two-phase slug flow. J. Heat Transf. 84, 29–38.

Nakoryakov, V., Kashinsky, O., Kozmenko, B., 1986. Experimental study of gas–liquid slug flow in a small-diameter vertical pipe. Int. J. Multiph. Flow 12, 337–355.

Nakoryakov, V., Kashinsky, O., Petukhov, A., Gorelik, R., 1989. Study of local hydrodynamic characteristics of upward slug flow. Exp Fluids 7, 560–566.

Nickens, H., Yannitell, D., 1987. The effects of surface tension and viscosity on the rise velocity of a large gas bubble in a closed, vertical liquid-filled tube. Int. J. Multiph. Flow 13, 57–69.

Nicklin, D., Wilkes, J., Davidson, J., 1962. Two-phase flow in vertical tubes. Trans. Inst. Chem. Eng. 40, 61–68.

Nikuradse, J., 1933. Laws of flow in rough pipes. VDi-Forschungsheft 361.

Nogueira, S., 2005. Flow around a single Taylor bubble rising through stagnant and co-current flowing newtonian liquids. Engenharia Química, PhD Thesis.

Nogueira, S., Riethmuler, M.L., Campos, J.B.L.M., Pinto, A.M.F.R., 2006a. Flow in the nose region and annular film around a Taylor bubble rising through vertical columns of stagnant and flowing Newtonian liquids. Chem. Eng. Sci. 61, 845–857.

Nogueira, S., Riethmuller, M., Campos, J., Pinto, A., 2006b. Flow patterns in the wake of a Taylor bubble rising through vertical columns of stagnant and flowing Newtonian liquids: an experimental study. Chem. Eng. Sci. 61, 7199–7212.

Nogueira, S., Sousa, R.G., Pinto, A.M.F.R., Riethmuller, M.L., Campos, J.B.L.M., 2003. Simultaneous PIV and pulsed shadow technique in slug flow: a solution for optical problems. Exp Fluids 35, 598–609.

Nusselt, W., 1916. Die Oberflachenkondesation des Wasserdamffes - the surface condensation of water. Zetrschr. Ver. Deutch. Ing. 60, 541–546.

Pavlidis, D., Xie, Z., Percival, J.R., Gomes, J.L., Pain, C.C., Matar, O.K., 2014. Two-and three-phase horizontal slug flow simulations using an interface-capturing compositional approach. Int. J. Multiph. Flow 67, 85–91.
Pering, T., Tamburello, G., McGonigle, A., Aiuppa, A., James, M., Lane, S.J., Sciotto, M., Cannata, A., Patanè, D., 2015. Dynamics of mild strombolian activity on Mt. Etna. J. Volcanol. Geothermal Res. 300, 103–111.
Pino, N.A., Moretti, R., Allard, P., Boschi, E., 2011. Seismic precursors of a basaltic paroxysmal explosion track deep gas accumulation and slug upraise. J. Geophys. Res.: Solid Earth 116.
Pinto, A., Campos, J., 1996. Coalescence of two gas slugs rising in a vertical column of liquid. Chem. Eng. Sci. 51, 45–54.
Pinto, A., Pinheiro, M.C., Campos, J., 2001. On the interaction of Taylor bubbles rising in two-phase co-current slug flow in vertical columns: turbulent wakes. Exp Fluids 31, 643–652.
Pinto, A.M.F.R., Coelho Pinheiro, M.N., Campos, J.B.L.M., 1998. Coalescence of two gas slugs rising in a co-current flowing liquid in vertical tubes. Chem. Eng. Sci. 53, 2973–2983.
Pinto, A.M.F.R., Coelho Pinheiro, M.N., Nogueira, S., Ferreira, V.D., Campos, J.B.L.M., 2005. Experimental study on the transition in the velocity of individual Taylor bubbles in vertical upward co-current liquid flow. Chem. Eng. Res. Des. 83, 1103–1110.
Polonsky, S., Barnea, D., Shemer, L., 1998. Image processing procedure for analysing the motion of an elongated bubble rising in a vertical pipe. In: Eighth International Symposium on Flow Visualisation.
Polonsky, S., Barnea, D., Shemer, L., 1999a. Averaged and time-dependent characteristics of the motion of an elongated bubble in a vertical pipe. Int. J. Multiph. Flow 25, 795–812.
Polonsky, S., Shemer, L., Barnea, D., 1999b. The relation between the Taylor bubble motion and the velocity field ahead of it. Int. J. Multiph. Flow 25, 957–975.
Portalski, S., 1963. Studies of falling liquid film flow film thickness on a smooth vertical plate. Chem. Eng. Sci. 18, 787–804.
Quan, S., 2011. Co-current flow effects on a rising Taylor bubble. Int. J. Multiph. Flow 37, 888–897.
Seyfried, R., Freundt, A., 2000. Experiments on conduit flow and eruption behavior of basaltic volcanic eruptions. J. Geophys. Res. 105, 23.
Shemer, L., 2003. Hydrodynamic and statistical parameters of slug flow. Int. J. Heat Fluid Flow 24, 334–344.
Shemer, L., Barnea, D., 1987. Visualization of the instantaneous velocity profiles in gas-liquid slug flow. Phys.-Chem. Hydrodyn. 8, 243–253.
Shemer, L., Gulitski, A., Barnea, D., 2005. Experiments on the turbulent structure and the void fraction distribution in the Taylor bubble wake. Multiph. Sci. Technol. 17 (1-2), 103–122.
Shemer, L., Gulitski, A., Barnea, D., 2007a. Movement of two consecutive Taylor bubbles in vertical pipes. Multiph. Sci. Technol. 19 (2), 99–120.
Shemer, L., Gulitski, A., Barnea, D., 2007b. On the turbulent structure in the wake of Taylor bubbles rising in vertical pipes. Phys. Fluids (1994-present) 19, 035108.
Sousa, R., Pinto, A., Campos, J., 2006. Effect of gas expansion on the velocity of a Taylor bubble: PIV measurements. Int. J. Multiph. Flow 32, 1182–1190.
Taha, T., Cui, Z., 2002. CFD modelling of gas-sparged ultrafiltration in tubular membranes. J. Membr. Sci. 210, 13–27.
Taha, T., Cui, Z.F., 2006. CFD modelling of slug flow in vertical tubes. Chem. Eng. Sci. 61, 676–687.
Taitel, Y., Barnea, D., 1990. Two-phase slug flow. Adv. Heat Transf. 20, 83–132.
Taitel, Y., Barnea, D., Dukler, A., 1980. Modelling flow pattern transitions for steady upward gas–liquid flow in vertical tubes. AIChE J. 26, 345–354.
Taitel, Y., Dukler, A., 1976. A model for predicting flow regime transitions in horizontal and near horizontal gas-liquid flow. AIChE J. 22, 47–55.
Talimi, V., Muzychka, Y., Kocabiyik, S., 2012. A review on numerical studies of slug flow hydrodynamics and heat transfer in microtubes and microchannels. Int. J. Multiph. Flow 39, 88–104.
Terrier, B., Courtois, D., Hénault, N., Cuvier, A., Bastin, M., Aknin, A., Dubreuil, J., Pétiard, V., 2007. Two new disposable bioreactors for plant cell culture: the wave and undertow bioreactor and the slug bubble bioreactor. Biotechnol. Bioeng. 96, 914–923.
Thome, J.R., 2015. Encyclopedia of Two-phase Heat Transfer and Flow I: Fundamentals and Methods (A 4-Volume set). World Scientific.
Tomiyama, A., Sou, A., Sakaguchi, T., 1996. Numerical simulation of a Taylor bubble in a stagnant liquid inside a vertical pipe. JSME Int. J. Ser. B Fluids Therm. Eng. 39, 517–524.
Tudose, E.-T., Kawaji, M., 1999. Experimental investigation of Taylor bubble acceleration mechanism in slug flow. Chem. Eng. Sci. 54, 5761–5775.
Tung, K.W., Parlange, J.-Y., 1976. Note on the motion of long bubbles in closed tubes-influence of surface tension. Acta Mech. 24, 313–317.
Van Hout, R., Barnea, D., Shemer, L., 2001. Evolution of statistical parameters of gas–liquid slug flow along vertical pipes. Int. J. Multiph. Flow 27, 1579–1602.
Van Hout, R., Barnea, D., Shemer, L., 2002a. Translational velocities of elongated bubbles in continuous slug flow. Int. J. Multiph. Flow 28, 1333–1350.
van Hout, R., Gulitski, A., Barnea, D., Shemer, L., 2002b. Experimental investigation of the velocity field induced by a Taylor bubble rising in stagnant water. Int. J. Multiph. Flow 28, 579–596.
Van Hout, R., Shemer, L., Barnea, D., 2003. Evolution of hydrodynamic and statistical parameters of gas–liquid slug flow along inclined pipes. Chem. Eng. Sci. 58, 115–133.
Viana, F., Pardo, R., Yanez, R., Trallero, J.L., Joseph, D.D., 2003. Universal correlation for the rise velocity of long gas bubbles in round pipes. J. Fluid Mech. 494, 379–398.
von Karman, T., 1939. The analogy between fluid friction and heat transfer. Trans. Am. Soc. Mech. Eng. 61, 705–710.
Wallis, G.B., 1969. One-Dimensional Two-phase Flow. McGraw-Hill, New York.
Wang, Y., Yan, C., Cao, X., Sun, L., Yan, C., Tian, Q., 2014a. Hydrodynamics of slug flow in a vertical narrow rectangular channel under laminar flow condition. Ann. Nucl. Energy 73, 465–477.
Wang, Y., Yan, C., Sun, L., Yan, C., 2014b. Characteristics of slug flow in a vertical narrow rectangular channel. Exp. Therm. Fluid Sci. 53, 1–16.
White, E.T., Beardmore, R.H., 1962. The velocity of rise of single cylindrical air bubbles through liquids contained in vertical tubes. Chem. Eng. Sci. 17, 351–361.
Yun, J., Shen, Z., 2003. Modeling of solid layer growth from melt for Taylor bubbles rising in a vertical crystallization tube. Chem. Eng. Sci. 58, 5257–5268.
Zhao, C.-X., Middelberg, A.P., 2011. Two-phase microfluidic flows. Chem. Eng. Sci. 66, 1394–1411.
Zukoski, E., 1966. Influence of viscosity, surface tension, and inclination angle on motion of long bubbles in closed tubes. J. Fluid Mech. 25, 821–837.